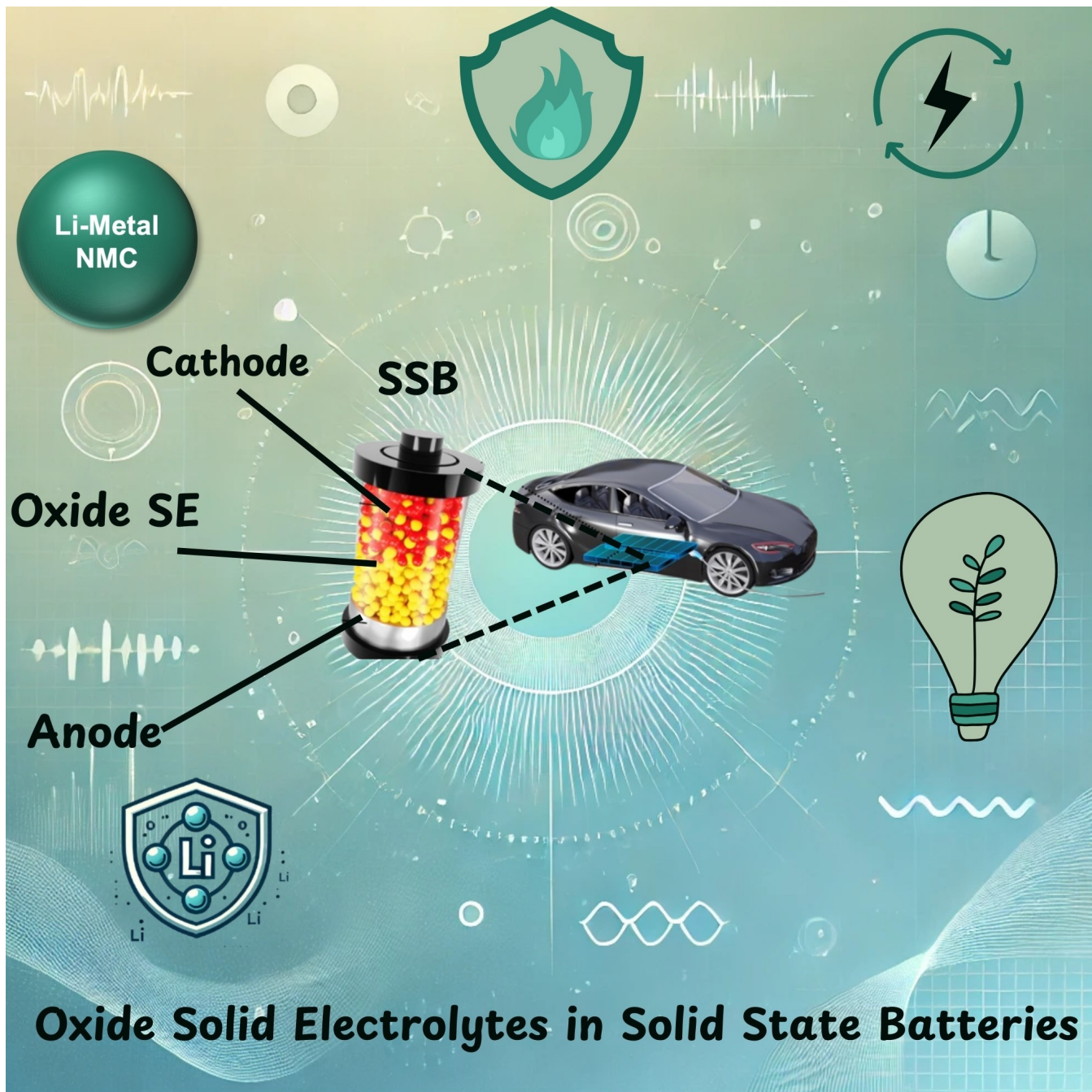


Oxide Solid Electrolytes in Solid-State Batteries

Muhammad Umair⁺^[a, b] Shiqiang Zhou⁺^[a, b] Wenzheng Li,^[a, b] Hafiz Talha Hasnain Rana,^[a, b] Jingyi Yang,^[a, b] Lukuan Cheng,^[a, b] Mengrui Li,^[a, b] Suzhu Yu,^{*[a, b]} and Jun Wei^{*[a, b, c]}



Solid-state electrolytes (SSEs) have re-emerged as high-priority materials for enhancing the safety and power density of electrochemical energy storage devices. However, several challenges, including low ionic conductivity, narrow redox windows, and interface issues, hinder the practical deployment of solid-state batteries (SSBs). In this review, we evaluate recent advances in the design, synthesis, and analysis of oxide SSEs and identify relevant structural and stability factors, as well as dimensional design concepts, for creating oxide SSEs to meet

practical application requirements. We provide an overview of the development and characteristics of oxide SSEs, then analyze bulk and ion transport based on different structures. We summarize the progress made in various synthetic approaches to oxide SSEs and discuss issues related to their stability and factors influencing ionic conductivity. Furthermore, we present the main challenges and future development directions of oxide SSBs to pave the way for the practical applications of oxide SSEs.

1. Introduction

In recent years, the pressing need to reduce greenhouse gas emissions has spurred the rapid growth of the global electric vehicle market and grid energy storage systems. This surge has, in turn, increased the demand for next-generation rechargeable batteries with high energy and power density.^[1–5] Lithium-ion batteries (LIBs) have gained popularity as power sources in various applications due to their significant energy and power densities, excellent coulombic efficiency, long cycle life, and minimal self-discharge characteristics.^[6,7] The SONY corporation introduced the first lithium-ion battery on the market in 1991. The past 32 years have witnessed significant advancements regarding LIBs.^[8,9] Conventional LIBs using combustible liquid electrolytes have inadequate energy density (250 Wh/kg and 600 Wh/L) and present potential safety risks, making it challenging to meet the growing energy demands of new applications.^[1,10–13] Lithium metal possesses the lowest electrical potential and the highest gravimetric energy density (−3.04 V vs standard hydrogen electrode, 3860 mAh g^{−1}), making it the preferred material as an anode for lithium-ion batteries. However, due to the strong reactivity between lithium metal and liquid electrolyte, some safety risks may arise, including thermal instability, explosion, and electrolyte leakage.^[7,14–18]

The SSBs that swap a liquid electrolyte with a solid electrolyte are recognized as an important rival. They not only demonstrate exceptional flame retardancy, high energy density, and outstanding chemical stability, but also provide a viable solution for safely meeting the needs of energy storage systems.^[12,19,20] The central component of a solid-state battery is the solid-state electrolyte (SSE), which includes certain ions with exceptional mobility that enable them to move across crystallographic locations and even function as fluid phases inside a

crystalline framework. The SSE serves as a practical separator that only permits the transport of lithium ions. SSEs are non-flammable, non-volatile, have superior mechanical strength, and are robust at extreme temperatures.^[4,21] The characteristics of an ideal SSE consist of minimal electronic conductivity, high lithium ion conductivity (> 1 mS/cm),^[22] wide electrochemical window, outstanding chemical interaction with electrodes, excellent thermal resilience,^[23] mechanical potency, low toxicity, and inexpensive for large-scale manufacturing.^[21]

In the past few decades several typical types of organic and inorganic SSEs, such as oxide, sulfide, metal halide, composite, and polymer, have been thoroughly investigated and significant advancements have been achieved in enhancing the aforementioned SSE features. Inorganic SSEs are preferred due to their excellent ionic conductivity, long cyclic life, safety, and temperature stability.^[24,25] Oxide solid electrolytes are inorganic SSEs that emerging as research hotspots in the current era due to superior ionic conductivity, exceptional mechanical features, significant thermal window, and outstanding safety profile with wide redox stable window.^[26,27] The development history of oxide solid electrolytes from the beginning to the present is displayed in Figure 1. SSLBs with oxide electrolytes deliver several incentives, such as increased energy density, improved security, and extended lifespan.^[28,29] Commercialization has been successful in different domains and is now being aggressively sought in others. SSLBs offer the promise to change consumer devices by enabling a longer lifespan of the battery, quicker charging, and greater safety. Smartphone companies, portable computing devices, and smartwatch businesses are manufacturing SSLBs for consumers.^[30] Owing to their outstanding energy density and safety features, SSLBs are being investigated for use in microelectronics, electric vehicles, as well as aerospace and defense applications.^[31,32]

Although oxide solid electrolytes offer great promise for SSLBs, a few important obstacles still stand in the way of their widespread use. A feature essential for battery life is obtaining high ionic conductivity remains one of the main challenges, numerous oxide electrolytes have lower ionic conductivities which must be higher for commercial feasibility. Furthermore, These materials frequently have stability issues, especially when it comes to the chemical relationship with Li electrodes, causing harmful interfacial interactions.^[27,33] A diversified strategy is needed to address these issues, one that incorporates the investigation of new materials, sophisticated synthesis methods, and creative interface engineering approaches. The purpose of this review is to shed light on these problems.

[a] M. Umair,⁺ S. Zhou,⁺ W. Li, H. T. H. Rana, J. Yang, L. Cheng, M. Li, S. Yu, J. Wei

School of Materials Science and Engineering, Harbin Institute of Technology (Shenzhen), Shenzhen 518055, China

E-mail: szyu@hit.edu.cn

junwei@hit.edu.cn

[b] M. Umair,⁺ S. Zhou,⁺ W. Li, H. T. H. Rana, J. Yang, L. Cheng, M. Li, S. Yu, J. Wei
Shenzhen Key Laboratory of Flexible Printed Electronics Technology, Harbin Institute of Technology (Shenzhen), Shenzhen 518055, China

[c] J. Wei

State Key Laboratory of Advanced Welding and Joining, Harbin Institute of Technology (Shenzhen), Shenzhen 518055, China

[+] These authors contributed equally to this work.

In this Review, we focus on the research progress of different types of oxide solid electrolytes, including design strategies based on structures, and synthesis methods. On this basis, factors influencing the ionic conductivity performances, the stability complications of oxide solid electrolytes for SSBs, and interface engineering are covered. Finally, we offer several

possible perspectives on the unresolved challenges and future opportunities for SSEs.



Muhammad Umair completed his Master's degree in Physics at the University of Agriculture, Faisalabad, Pakistan. He is currently a Ph.D. candidate under the supervision of Prof. Jun Wei at the Shenzhen Key Laboratory of Flexible Printed Electronics, Harbin Institute of Technology, Shenzhen. His research focuses on developing and optimizing solid-state electrolytes for lithium-ion batteries.



Shiqiang Zhou received his master's degree from National Center for International Research on Photoelectric and Energy Materials, Yunnan University. He is now a PhD candidate under Prof. Jun Wei supervision in the Shenzhen Key Laboratory of Flexible Printed Electronics Technology Center, Harbin Institute of Technology, Shenzhen. His current research mainly focuses on using different printing methods to fabricate solid-state lithium-ion batteries.



Wenzheng Li graduated with a master's degree from Harbin Institute of Technology, Shenzhen, and he is currently a doctoral student at the Flexible Electronic Printing Center of Harbin Institute of Technology, Shenzhen, whose research direction is the design of solid-state lithium-ion battery electrolytes.



Hafiz Talha Hasnain Rana received his Master's degree in Physics from the University of Agriculture, Faisalabad, Pakistan. He is currently pursuing his Ph.D. under the supervision of Prof. Jun Wei at the Shenzhen Key Laboratory of Flexible Printed Electronics, Harbin Institute of Technology, Shenzhen. His research primarily focuses on flexible lithium-ion batteries.



Jingyi Yang received her bachelor's degree from School of Materials Science and Engineering, Dalian University of Technology. She is now a Master's candidate under Prof. Jun Wei's supervision in the Shenzhen Key Laboratory of Flexible Printed Electronics Technology Center, Harbin Institute of Technology. Her current research mainly focuses on polymer/inorganic composite solid-state electrolytes.



Mengrui Li received her master's degree from College of Bioresources Chemical & Materials Engineering, Shaanxi University of Science and Technology. Since 2021, she has been pursuing her Ph.D. degree at School of Materials Science and Engineering, Harbin Institute of Technology Shenzhen under the supervision of Prof. Jun Wei. Her research interest mainly focuses on the design and fabrication of 3D printed energy storage devices, and the related mechanism.



Lukuan Cheng is currently a Ph.D candidate under the supervision of Prof. Jun Wei at Harbin Institute of Technology, Shenzhen. He received his Bachelor's degree in school of Material Science and Engineering from Harbin Institute of Technology, 2020. He obtained his Master's degree in school of Material Science and Engineering from Harbin Institute of Technology, 2023. His research interests focus on novel electrode and separator materials for high-performance Li/Zn-ion batteries.



Suzhu Yu is a professor at School of Materials Science and Engineering, Harbin Institute of Technology (Shenzhen). She received her PhD from Nanyang Technological University of Singapore and appointed as a Scientist at Singapore Institute of Manufacturing Technology prior to the current position. Her research focuses on additive manufacturing, flexible printed electronics, and functional materials development. She has led a number of research and industry projects, and published more than 100 papers.



Jun Wei is the professor in Harbin Institute of Technology (Shenzhen). Concurrently he is the University President Assistant, Director of Shenzhen Key Laboratory of Flexible Printed Electronics Technology, Director of Flexible Printed Electronics Center. Before this appointment, he was the Principal Scientist and Director of Research Liaison Office in Singapore Institute of Manufacturing Technology (SIMTech), the Additive Manufacturing Programme Manager for the Agency for Science, Technology and Research (A*STAR). Dr Wei's research includes additive manufacturing, and flexible printed electronics. He has authored and co-authored over 800 publications with citations over 2700 times and H-index of 82.

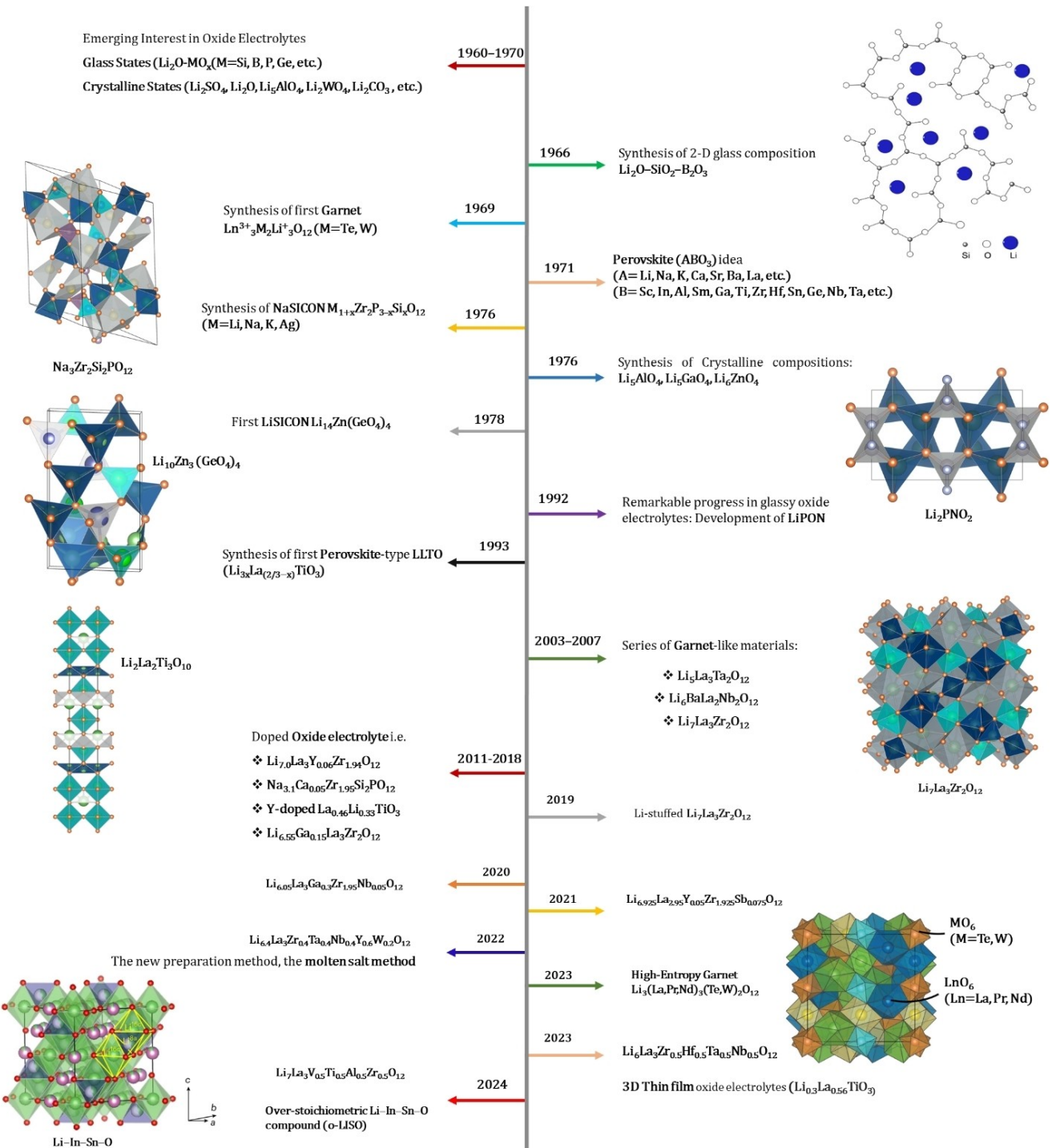


Figure 1. Development history of oxide solid electrolytes from the beginning to the present.

2. Research Advancement in Oxide Solid Electrolytes

To date, extensive research has been conducted on oxide solid electrolytes, with ongoing efforts continuing to expand our understanding. Inorganic solid-state electrolytes can be classified into a broad family of sulfide and oxide-based series. In various applications, oxide-based SSEs prove superior to sulfide-

based ones. Notably, oxide-based SSEs often exhibit greater chemical stability compared to sulfides. When addressing dendritic development and thermal instability, oxide-based electrolytes tend to outperform sulfide-based ones. Additionally, oxide SSEs operate over a broader temperature range than sulfides, making them suitable for industries such as aerospace and automotive, where temperature fluctuations are common.^[14,21] Herein Oxide SSEs, consisting of garnet-type,

NaSICON-type, LiSICON-type, and perovskite-type, will be discussed in the following sections. The characteristic crystalline structures for all types are displayed in Figure 2. The four different oxide SSEs, perovskite, garnet, NaSICON, and LiSICON have unique structural and electrochemical features.^[34] Garnet-type electrolytes exhibit excellent ionic conductivity due to their cubic crystal structure, making them ideal for SSLBs as they are highly stable with Li^+ . NaSICON electrolytes, with their 3D structure, demonstrate exceptional stability in the atmosphere and significantly high ionic conductivity. LiSICON electrolytes are known for their good thermal stability. Perovskite-type electrolytes, on the other hand, are highly stable in air and exhibit excellent bulk ionic conductivity.^[35,36] They exhibit improved chemical durability and increased oxidation stability when paired with oxide cathodes,^[37] possess a broad operational temperature range, and demonstrate excellent stability under various environmental conditions, highlighting their high level of safety.^[38] The summary of different oxide solid electrolyte materials with ionic conductivity, crystal structure, and synthesis method is shown in Table 1.

2.1. Garnet Type

The garnet-type material exhibits a general chemical makeup of $\text{A}_3\text{B}_2(\text{XO}_4)_3$ and holds a face-centered cubic structure. A, B, and X are coordinated cation sites with 8, 6, and 4 oxygen atoms respectively.^[9,74] In the ideal garnets A=(any rare earth or Mg, Ca), B=(Zr, Fe, Al, Ni, V, Cr), and X=(Si, Ge).^[75] The interconnecting vacant polyhedral spots in the garnet-type framework constitute a potential lithium conductor if the X site in this

framework is grabbed by Li.^[10] Many garnet-type electrolytes, frequently referred to as Lithium-rich garnet, usually incorporate V-VII Li atoms in each structure.^[76] Garnet-type electrolytes can be categorized into multiple classes according to the calculation for lithium content. These groups consist of the Li (III) series, $\text{Li}_3\text{Ln}_3\text{Te}_2\text{O}_{12}$,^[77] Li (V) series, $\text{Li}_5\text{La}_3\text{M}_3\text{O}_{12}$,^[39] Li (VI) series, $\text{Li}_6\text{Al}_2\text{M}_2\text{O}_{12}$,^[78] and L (VII) series, $\text{Li}_7\text{La}_3\text{M}_2\text{O}_{12}$.^[79] A thorough investigation shows that the lithium coordination framework of the garnet structure is closely connected to the improved Li-ion conductivity. Cussen reported that lithium-ions in garnet frameworks are dispersed in three distinct intermittent sites 1) tetrahedral (24 d), 2) octahedral (48 g), and 3) tilted octahedral (96 h).^[80] In the Li (III) series all 3 Li atoms hold 24 d tetrahedral locations, however, the additional Li ions that are subsequently induced in the Li (V)-Li (VII) series hold octahedral positions. Two further subgroups of the Li (VII) series were discovered: tetrahedral LLZO in the $I4_1/acd$ space group having fully arranged lithium occupancy, and cubic LLZO in the $Ia-3d$ space group with completely disordered lithium layout, that's why cubic LLZO exhibits higher Li-ion conductivity. In the octahedral site, Li shows easy transport but the tetrahedral site fails, the observed Li-ion conductivity and the Li % in the octahedral arrangement are closely correlated.^[10] Garnet-type oxide electrolytes exhibit a broad electrochemical potential range and illustrate the most significant overall lithium-ion conductivity than other oxide-based SSEs, which makes them a suitable candidate for developing high-energy density battery packs with the contribution of a 5 V-type cathode and the lithium metal anode.^[81]

The first garnet-type compound with a composition of $\text{Li}_5\text{La}_3\text{M}_2\text{O}_{12}$ (where M=Ta, Nb) was reported in 2003 by

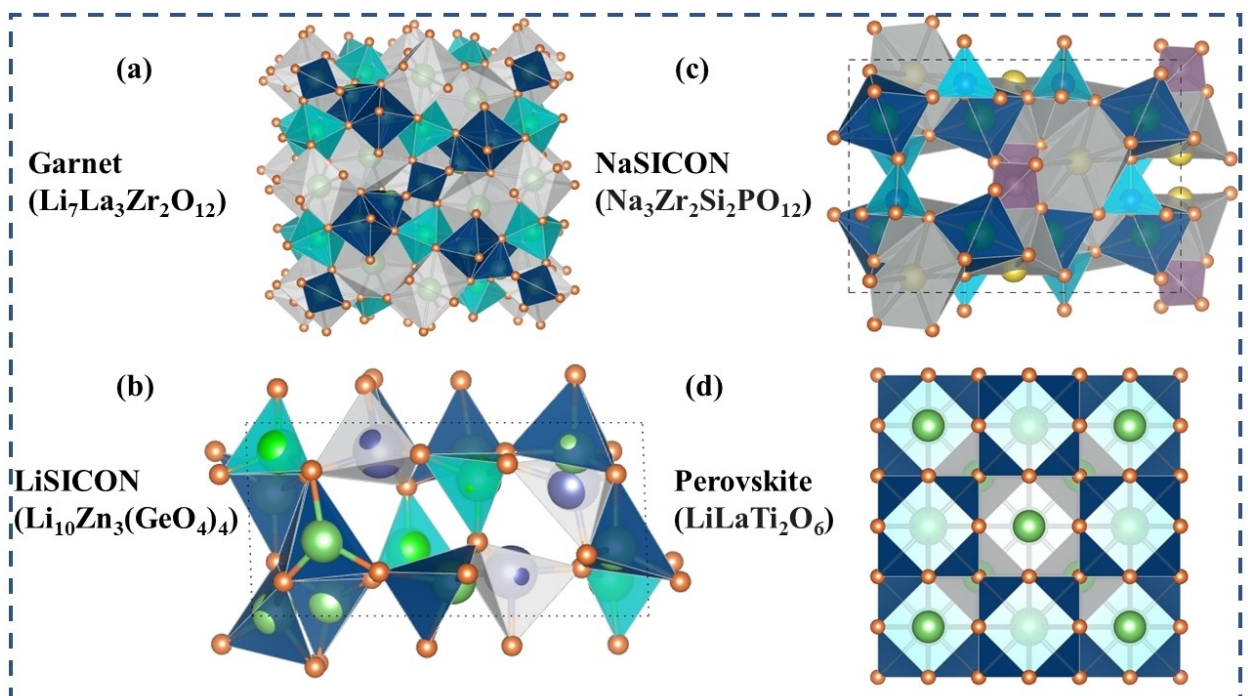


Figure 2. Characteristic crystalline structures: (a) Garnet, (b) NaSICON, (c) LiSICON, and (d) Perovskite.

Table 1. The summary of different oxide solid electrolyte materials with ionic conductivity, crystal structure, and synthesis method.

Type	Composition	σ [S/cm]	σ [$^{\circ}$ C]	Structure	Synthesis	Ref.
Garnet	$\text{Li}_5\text{La}_3\text{Ta}_2\text{O}_{12}$	1.54×10^{-6}	25	Cubic	Sol-gel	[39]
	$\text{Li}_5\text{La}_3\text{Zr}_2\text{O}_{12}$	2.0×10^{-4}	30	Cubic	Co-precipitation	[40]
	$\text{Li}_7\text{La}_3\text{Zr}_2\text{O}_{12}$	2.44×10^{-4}	25	Cubic	Solid-state	[41]
	$\text{Li}_{7-x}\text{La}_3\text{Zr}_{2-x}\text{Ta}_x\text{O}_{12}$	1×10^{-3}	25	Cubic	Solid-state	[42]
	$\text{Te-Li}_7\text{La}_3\text{Zr}_2\text{O}_{12}$	1.02×10^{-3}	25	Cubic	Solid-state	[43]
	$\text{Li}_{6.55+y}\text{Ga}_{0.15}\text{La}_3\text{Zr}_{2-y}\text{Sc}_y\text{O}_{12}$	1.8×10^{-3}	27	Cubic	Sol-gel	[44]
	$\text{Li}_{6.55}\text{Ga}_{0.15}\text{La}_3\text{Zr}_2\text{O}_{12}$	2.06×10^{-3}	25	Cubic	Solid-state	[45]
	$\text{Li}_{6.05}\text{La}_3\text{Ga}_{0.3}\text{Zr}_{1.95}\text{Nb}_{0.05}\text{O}_{12}$	9.28×10^{-3}	25	Cubic	Sol-gel	[46]
	$\text{Li}_{6.05}\text{La}_3\text{Zr}_{0.5}\text{Hf}_{0.5}\text{Ta}_{0.5}\text{Nb}_{0.05}\text{O}_{12}$	3.3×10^{-3}	25	Cubic	Solid-state	[47]
	$\text{Li}_7\text{La}_3\text{Zr}_{0.5}\text{Nb}_{0.5}\text{Ta}_{0.5}\text{Hf}_{0.5}\text{O}_{12}$	4.67×10^{-4}	25	Cubic	Solid-state	[48]
NaSICON	$\text{Na}_3\text{Zr}_2\text{Si}_2\text{PO}_{12}$	1.13×10^{-3}	20	Monoclinic	Solid-state	[49]
	$\text{Na}_{3.1}\text{Zr}_{1.95}\text{Mg}_{0.05}\text{Si}_2\text{PO}_{12}$	3.5×10^{-3}	25	Monoclinic	Solid-state	[50]
	$\text{Ca}^{2+}-\text{Na}_3\text{Zr}_2\text{Si}_2\text{PO}_{12}$	1.67×10^{-3}	25	Monoclinic	Sol-gel	[51]
	$\text{Na}_{3.3}\text{Zr}_{1.7}\text{La}_{0.3}\text{Si}_2\text{PO}_{12}$	6.7×10^{-3}	25	Monoclinic	Solid-state	[52]
	$\text{Na}_{3.55}\text{Zr}_{1.85}\text{Al}_{0.15}\text{Si}_{2.40}\text{P}_{0.60}\text{O}_{12}$	2.1×10^{-3}	25	Monoclinic	Sol-gel	[53]
	$\text{Na}_{3.33}\text{Zr}_{1.67}\text{Sc}_{0.29}\text{Yb}_{0.04}\text{Si}_2\text{PO}_{12}$	1.62×10^{-3}	25	Rho/Mono.	Solid-state	[54]
	$\text{LiTi}_2(\text{PO}_4)_3$	2×10^{-6}	25	Rhombohedral	Solid-state	[55]
	$\text{LiGe}_2(\text{PO}_4)_3$	6.62×10^{-9}	25	Rhombohedral	Solid-state	[55]
	$\text{Li}_{1.3}\text{Al}_{0.3}\text{Ti}_{1.7}(\text{PO}_4)$	7×10^{-4}	25	Rhombohedral	Solid-state	[56]
	$\text{Li}_{1.3}\text{Al}_{0.3}\text{Ti}_{1.7}(\text{PO}_4)_3$	6.39×10^{-4}	25	Rhombohedral	Sol-gel	[57]
	$\text{Li}_{1.5}\text{Al}_{0.5}\text{Ge}_{1.5}(\text{PO}_4)_3$	3.5×10^{-6}	25	Rhombohedral	Solid-state	[58]
	$\text{Li}_{1.5}\text{Al}_{0.4}\text{Cr}_{0.1}\text{Ge}_{1.5}(\text{PO}_4)_3$	6.65×10^{-3}	25	Rhombohedral	Melt-quenching	[59]
LiSICON	$\text{Li}_{3.6}\text{Ge}_{0.6}\text{V}_{0.4}\text{O}_4$	4.00×10^{-5}	18	Orthorhombic	Solid-state	[60]
	$\text{Li}_{3.5}\text{Si}_{0.5}\text{P}_{0.5}\text{O}_4$	1.31×10^{-7}	25	Tetrahedral	Solid-state	[61]
	$\text{Li}_{2+2x}\text{Zn}_{1-x}\text{Ge}_x\text{O}_4$	3.90×10^{-7}	25	Tetragonal	Solid state	[62]
	$\text{Li}_{3+x}\text{Cr}_{1-x}\text{Ge}_x\text{O}_4$	1.40×10^{-5}	25	orthorhombic	Solid state	[63]
	$\text{Li}_{10.42}\text{Si}_{1.5}\text{P}_{1.5}\text{Cl}_{0.08}\text{O}_{11.92}$	1.03×10^{-5}	27	Orthorhombic	Solid-state	[64]
	$\text{Li}_{10.42}\text{Ge}_{1.5}\text{P}_{1.5}\text{Cl}_{0.08}\text{O}_{11.92}$	3.7×10^{-5}	27	Orthorhombic	Solid-state	[64]
	$\text{Li}_{3.53}(\text{Ge}_{0.75}\text{P}_{0.25})_{0.7}\text{V}_{0.3}\text{O}_4$	5.1×10^{-5}	25	Orthorhombic	Solid-state	[65]
	$\text{Li}_4\text{Al}_{1/3}\text{Si}_{1/6}\text{Ge}_{1/6}\text{P}_{1/3}\text{O}_4$	9×10^{-4}	25	Monoclinic	Solid-state	[66]
Perovskite	$\text{Li}_{0.34}\text{La}_{0.51}\text{TiO}_{2.94}$	2×10^{-5}	25	Cubic	Solid state	[67]
	$\text{LiSr}_{1.65}\text{Ti}_{1.3}\text{Ta}_{1.0}\text{O}_9$	4.99×10^{-5}	30	Cubic	Solid state	[68]
	$\text{Li}_{2x-y}\text{Sr}_{1-x}\text{Ta}_x\text{Zr}_{1-y}\text{O}_3$	2.7×10^{-4}	27	Cubic	Solid-state	[69]
	$\text{Li}_{3/8}\text{Sr}_{7/16}\text{Hf}_{1/4}\text{Ta}_{3/4}\text{O}_3$	3.8×10^{-4}	25	Cubic	Solid-state	[70]
	$\text{Li}_{0.38}\text{La}_{0.56}\text{Ti}_{0.99}\text{Al}_{0.01}\text{O}_3$	3.17×10^{-4}	25	Tetragonal	Sol-gel	[71]
	$\text{Li}_{0.33}\text{La}_{0.46}\text{Y}_{0.1}\text{TiO}_3$	8.03×10^{-5}	25	Cubic	Sol-gel	[72]
	$\text{Li}_{0.25}\text{La}_{0.66}\text{Ti}_{0.75}\text{Al}_{0.25}\text{O}_3$	7.66×10^{-5}	25	Cubic	Solid-state	[73]

Thangadurai et al.^[82] In 2007, a further comprehensive investigation was conducted by Murugan et al.,^[79] They prepared a famous garnet-type cubic $\text{Li}_5\text{La}_3\text{Zr}_2\text{O}_{12}$ solid-state electrolyte that exhibits outstanding ionic conductivity (0.24 mS cm^{-1}) at room temperature which was greater than other previously documented Li garnet-type materials and it was successfully demonstrated that this structure could accommodate seven lithium ions.^[3,9,22,74] Several garnet-type SSEs have been manufactured, however, a particular group of oxide SSEs, the $\text{Li}_5\text{La}_3\text{Zr}_2\text{O}_{12}$ (LLZO) garnet-type is noteworthy owing to its: i) Relatively strong ionic conductivity (0.1 mS cm^{-1} – 1 mS cm^{-1}),^[13] adjustable by doping components up to 9.28 mS cm^{-1} at 25°C temperature, ii) Processing ability in the air, 3) a substantial shear elasticity relative to Li to stabilize the anode contact mechanically, and iv) broad electrochemical reliability window. Since it is a ceramic, LLZO offers unparalleled stability even at elevated operational temperatures and can further improve safety if utilized in conjunction with other SEs.^[45,46,83] This Li-rich electrolyte is also considered the foremost promising due to its minimal electron conductivity.^[9] Li-rich LLZO exhibits both cubic and tetragonal phases in its structures. When the temperature at which sintering occurs increases, the crystal geometry

transitions from a tetragonal to a cubic phase.^[13,24,84] Approximately two orders greater ionic conductivity is observed in the cubic phase as compared to the tetragonal phase structure.^[85]

The garnet material's mechanical characteristics, which are influenced by several variables including temperature, flaws, and microstructure, describe how the material reacts to stress. The mechanical features of Li-rich garnet material ($\text{Li}_{6.4}\text{Al}_{0.24}\text{La}_3\text{Zr}_2\text{O}_{11.98}$) were first reported by Ni et al.,^[86] they stated that the material shear modulus is $\sim 60 \text{ GPa}$ and Young's modulus is $\sim 150 \text{ GPa}$. Whereas, Li metal exhibits Young's and shear moduli of 4.9–13 and 4–5 GPa, respectively.^[87] The Li-garnets exhibit an order of scale greater shear modulus as compared to Li metal, and due to their substantial Li transference numbers, garnet-type LLZO SEs were anticipated to be capable of inhibiting the formation of Li dendrites. Ceramic garnet-type materials are considered to have a knack for acting as separators to obstruct Li dendrite in Li-metal batteries due to their stiff character.^[88] It is commonly known that solid electrolytes of the garnet type are stable, compatible with Li metal, and stable during oxidation at elevated voltages. Cyclic voltammetry measurements have been used to study the oxidation durability of garnet solid electrolytes. Due to their

large electrochemical window (>6 V vs Li/Li $^{+}$), garnet SSEs represent the most robust SSEs for Li metal anode/cathode materials, allowing for the development of exceptionally high-voltage batteries.^[89] Garnet electrolytes are renowned for their great safety thanks to their long-lasting nature and minimal reactivity with other substances. To guarantee the security of lithium-ion batteries, these are important.^[38]

2.2. NaSICON Type

The generic formula for sodium-super-ionic-conductors (NaSICON) type SSEs ($\text{Na}_{1+x}\text{Zr}_2\text{Si}_x\text{P}_{3-x}\text{O}_{12}$) was presented in 1976 for the first time by Goodenough et al.^[90] and Hong.^[91] This general formula was derived from $\text{AM}_2(\text{PO}_4)_3$, where A is typically occupied by Li, Na, or K, and Ge, Zr, or Ti is generally occupied by M.^[92] All compositions between ($0 \leq x \leq 3$), the NaSICON class of materials having standard formula $\text{Na}_{1+x}\text{Zr}_2\text{Si}_x\text{P}_{3-x}\text{O}_{12}$ forms rhombohedral structure containing the R-3 C space group, however, for compositions between ($1.8 \leq x \leq 2.2$), it crystallizes in a monoclinic phase having the space group C2/c at room temperature.^[93] When the Si content rises to $1.8 \leq x \leq 2.2$, it changes to a monoclinic symmetry. Afterward, it returns to the rhombohedral structure, further raising the Si concentration.^[94,95] In addition, the shear deformation of the unit cell around (420–450 K) may cause the monoclinic NaSICON structure to change into a rhombohedral.^[96] Built upon a stiff skeleton, MO₆ octahedra and PO₄ tetrahedra are connected by sharing corner oxygen atoms in a single building unit, forming the basic structure of the NaSICON-type SSE, these tetrahedron and octahedron share the routes for diffusion of ions.^[10,24] A lot of research reported on NaSICON-type electrolytes exhibiting $\text{Na}_3\text{Zr}_2\text{Si}_2\text{PO}_{12}$ series and monoclinic NaSICON structures demonstrates more effective ionic conductivity at room temperature over rhombohedral NaSICON structure because it has a wide unit-cell size, improved sodium ion relationships, and lowered energy obstacles for Na-ion conduction.^[93] The $\text{Na}_3\text{Zr}_2\text{Si}_2\text{PO}_{12}$ possesses an average activation energy of 0.36 eV and limited ionic conductivity of 0.67 mS cm $^{-1}$ at room temperature.^[97,98] However, interestingly in 2021 Narayanan et al., (2019) obtained the highest ionic conductivity (1.13 mS cm $^{-1}$ at 20 °C) for $\text{Na}_3\text{Zr}_2\text{Si}_2\text{PO}_{12}$.^[49]

Based on the composition of various elements, NaSICON-type electrolytes could be categorized into three main groups: (i) $\text{LiZr}_2(\text{PO}_4)_3$ (LZP), (ii) $\text{LiTi}_2(\text{PO}_4)_3$ (LTP), and (iii) $(\text{LiGe}_2(\text{PO}_4)_3$ (LGP). Compared to LZP, the ionic conductivity of LTP and LGP is substantially superior. The most extensively researched compounds in the NaSICON family are $\text{LiTi}_2(\text{PO}_4)_3$ and $\text{LiGe}_2(\text{PO}_4)_3$. It demonstrated from reported literature that selective substitution of Ti $^{4+}$ /Ge $^{4+}$ ions by trivalent and divalent cation ions, such as (Al, Ga, Sc, In, Y, La, Fe, Cr, Zn, and Ca) significantly increases the ionic conductivity in $\text{LiTi}_2(\text{PO}_4)_3$ and $\text{LiGe}_2(\text{PO}_4)_3$ networks. Aluminum (Al) doping is an especially efficient way to increase the ionic conductivity of the solid electrolyte than other dopants.^[14,99] The $\text{Li}_{1+x}\text{Al}_x\text{Ti}_{2-x}(\text{PO}_4)_3$ (LATP), and $\text{Li}_{1+x}\text{Al}_x\text{Ge}_{2-x}(\text{PO}_4)_3$ (LAGP) possess good electrochemical security, inexpensive cost, low toxicology, and are

chemically stable in air and water, they are also simple to prepare. Additionally, at ambient temperature, they display appealing ionic conductivities of 10^{-4} – 10^{-3} S cm $^{-1}$.^[100] The greatest recorded ionic conductivity is ($\sigma \approx 3$ mS/cm) for $\text{Li}_{1.3}\text{Al}_{0.3}\text{Ti}_{1.7}(\text{PO}_4)_3$ at room temperature and the reported $\text{Li}_x\text{Al}_x\text{Ge}_{2-x}(\text{PO}_4)_3$ material exhibited significantly improved ionic conductivity of 5 mS cm $^{-1}$.^[9] Due to the significant ionic radius imbalance, the level of substitution is restricted to (~15%, $x = 0.3$) exceeding this point, an additional phase of Al $^{3+}$ or Sc $^{3+}$ forms, and ionic conductivity subsequently decreases.^[56] The $\text{Li}_{1.4}\text{Al}_{0.4}\text{Ti}_{1.6}(\text{PO}_4)_3$ shows ionic conductivity of 1.09 mS cm $^{-1}$ was reported.^[24] Additionally, glass-ceramic-type LATP and LAGP have shown potential in reducing the lithium transportation resistance at grain boundaries.^[101,102] That's why, the ceramic-glass pellet samples $\text{Li}_{1.5}\text{Al}_{0.4}\text{Cr}_{0.1}\text{Ge}_{1.5}(\text{PO}_4)_3$ especially demonstrated the highest ionic conductivity of 6.65 mS cm $^{-1}$.^[59] The mechanical characteristics of NaSICON are generally unsatisfactory due to their low fracture resilience as well as elevated elastic modulus, which range from 115 GPa for LATP to 125 GPa for LAGP.^[1]

2.3. LiSICON Type

Lithium-super-ionic-conductors have been shortened as (LiSICON) $\text{Li}_{14}\text{Zn}(\text{GeO}_4)_4$ was first reported by Hong et al.^[103] in 1978. In the general formula ($\text{Li}_{16-2x}\text{A}_x(\text{BO}_4)_4$) x ranges between ($0 < x < 4$), A symbolizes the divalent cation (Zn $^{2+}$ or Mg $^{2+}$) and B denotes the tetravalent (Ge $^{4+}$ or Si $^{4+}$). The LiSICON orthorhombic crystalline structure with space group Pnma looks similar to $\gamma\text{-Li}_3\text{PO}_4$. Li ions are distributed at four distinct locations in the $\text{Li}_{14}\text{Zn}(\text{GeO}_4)_4$ unit cell, four hold 4c sites, seven occupy 8d locations, and the last three are distributed at the 4c and 4a spots. $\text{Li}_{14}\text{Zn}(\text{GeO}_4)_4$ exhibits ionic conductivity 1.25×10^{-1} S cm $^{-1}$ at 300 °C, while at room temperature it is 10^{-4} mS cm $^{-1}$.^[104,105] Due to its distinct crystal structure, particularly facilitating the quick transfer of high concentrations of Li $^{+}$ ions, it has excellent ion conductivity at elevated temperatures. A three-dimensional lithium transport channel may be formed inside the basic framework of $(\text{Li}_{11}\text{ZnGe}_4\text{O}_{16})^{3-}$, where the positions 4c and 8d are occupied by 11 Li $^{+}$ ions. The framework's interstitial locations 4a and 4c hold three movable lithium ions. and partially octahedral site vacancy promotes lithium conduction to a greater extent.^[10,105]

To enhance Li $^{+}$ ion movement, intervening solid solutions with a γ -tetrahedron geometry are essential. Kuwano et al. (1980) synthesized a novel LiSICON kind ($\text{Li}_{3+x}\text{Ge}_x\text{V}_{1-x}\text{O}_4$) that possessed excellent ionic conductivity at 18 °C is 4×10^{-2} mS cm $^{-1}$. $\text{Li}_{3+x}\text{Ge}_x\text{V}_{1-x}\text{O}_4$ exhibits the identical structure as $\gamma_{II}\text{-Li}_3\text{PO}_4$, representing a solid solution that lies within $\gamma_{II}\text{-Li}_3\text{VO}_4$ and Li_4GeO_4 . Li $^{+}$ and Ge $^{4+}$ replace a portion of the V $^{5+}$ in the $\gamma_{II}\text{-Li}_3\text{VO}_4$ and the extra Li $^{+}$ ions fill the interstices positions to create interstice lithium ions in the $\text{Li}_{3+x}\text{Ge}_x\text{V}_{1-x}\text{O}_4$ crystal structure. The thermal resistance and near-zero vapor pressure of LISICONs enable them to function at high temperatures, and they are resistant to water. However, the primary disadvantage is often linked to extreme reactivity with lithium metals and

poor ionic conductivity at ambient temperatures around 10^{-4} S cm $^{-1}$ but selective replacement could result in improved Li-ion conductivity. In summary, the ionic conductivity of LISICON solid electrolytes demonstrated inadequate usefulness in ASSBs.^[1,106]

2.4. Perovskite Type

The perovskite-type materials reported by Takahashi and Iwahara in 1971^[107] with the ABO₃ formula, Here A and B represent 6 and 12 oxygen-coordinated cation sites respectively. The (Li, Na, K, Ca, Sr, Ba, La, etc.) cations with high ionic radii can occupy the A site. However, cations with smaller ionic radii such as (Sc, In, Al, Sm, Ga, Ti, Zr, Hf, Sn, Ge, Nb, Ta, etc.) can occupy the B site. The two basic crystal configurations observed in perovskite Li-ion SEs are tetragonal and cubic perovskites.^[108] The first perovskite-type solid electrolyte lithium lanthanum titanate (LLTO) with the general formula Li_{3x}La_(2/3-x)TiO₃ was developed by Inaguma et al.^[67] Generally speaking, the two primary forms of crystal structures, cubic and tetragonal observed in perovskite-type electrolytes because they are A-site-sufficient materials. According to the previous research investigations, the four oxide series [(Li, Sr)(B, B') where, (B'=Ta, Nb, etc. and B=Hf, Ti, Sn, Zr, Ga, etc.)], present cubic crystal structure and nearly all LLTO compounds exhibit a tetragonal structure. The octahedral avenues of the cubic perovskite framework exhibit a uniform distribution of A-site ions and vacant positions. In contrast, the tetragonal structure exhibits an uneven distribution of La₃ at La₁ and La₂ locations. This is believed to be the primary cause of the doubled level of the c-axis cell parameters and the slanting of the TiO₆ octahedra. Furthermore, the La-rich and La-poor layers have been designated as La₁ and La₂ layers, correspondingly. The Li-ion fills the A-site in the LLTO structure due to lower activation energy than the 3c sites.^[108–111] The cubic LLTO exhibits strong Li⁺ conductivity as a result of its vacancies, which permit Li⁺ ions to move using a vacancy pathway as well as a square-planar bottleneck created by four O₂ ions that separate two adjacent A sites.^[38]

At ambient temperature, perovskites typically exhibit lower electronic conductivity (10^{-8} S cm $^{-1}$) and comparatively elevated lithium-ion conductivities range between 10^{-3} – 10^{-4} S cm $^{-1}$. The LLTO (Li_{0.34(1)}La_{0.51(1)}TiO_{2.94(2)}) SSE reported by Inaguma et al. (1993) exhibit bulk and total ionic conductivity of 1 mS cm $^{-1}$ and 2×10^{-2} mS cm $^{-1}$ respectively.^[67,112] In 1994, Harada et al. reported the bulk ionic conductivity of 1.53 mS cm $^{-1}$ at 25 °C for cubic La_{0.67-x}Li_{3x}TiO₃ ($x = 0.06\text{--}0.15$).^[113] Li_{3/8}Sr_{7/16}Ta_{3/4}Zr_{1/4}O₃ was determined to possess the greatest ionic conductivity by Chen et al. 2004^[114] with bulk and grain boundary values of 2×10^{-1} mS cm $^{-1}$ and 1.33×10^{-1} mS cm $^{-1}$ respectively at 30 °C. It is one scale greater than LLTO, resulting in stronger overall ionic conductivity although its bulk ionic conductivity is one scale lower. Thangadurai et al. (1999) reported cubic LiSr_{1.65}Ti_{1.3}Ta_{1.7}O₉ material with a total ionic conductivity of 4.99×10^{-2} mS cm $^{-1}$ at 30 °C.^[68] In 2014, another Li_{2x-y}Sr_{1-x}Ta_yZr_{1-y}O₃ series prepared by Inada et al. possessed a total ionic conductivity value of

2.7×10^{-1} mS cm $^{-1}$ at 27 °C.^[69] Huang et al. (2016) synthesized Li₃-Sr_{7/16}Ta_{3/4}Hf_{1/4}O₃ by substituting Hf for Zr, the ionic conductivity was greater than Li_{2x-y}Sr_{1-x}Ta_yZr_{1-y}O₃ measuring 3.8×10^{-1} mS cm $^{-1}$ at 25 °C.^[70] In 2017, Kwon et al. synthesized lithium excess Li_{0.22}La_{0.60}TiO₃ showing the improved total ionic conductivity of 4.8×10^{-1} mS cm $^{-1}$ at ambient temperature.^[115] Lee et al. (2019) prepared Y-doped La_{0.46}Li_{0.33}TiO₃ electrolyte materials with a total ionic conductivity value of 8.03×10^{-2} mS cm $^{-1}$ at room temperature.^[72] Perovskite-type materials are thought to be generally good options for all SSEs due to their suitable ionic conductivities as well as acceptable electrochemical windows. However, When Ti⁴⁺ interacts with metal lithium, it reduces to Ti³⁺ which limits the applicability of LLTO even with its strong ionic conductivity at ambient temperature, suitable electrochemical window, and excellent oxidation stability. The perovskite-type materials are hard, their reported elastic modulus is 200 GPa.^[1,3,22,38]

3. Synthesis Mechanisms

Oxide-based solid electrolytes, as part of inorganic solid electrolytes, share similar preparation and synthesis processes, with common objectives such as phase stabilization, enhancement of ionic conductivity, density improvement, impedance reduction, and low-temperature sintering. This section will discuss the fundamental methods for manufacturing solid oxide electrolytes in both bulk and thin film forms. Figure 3 illustrates the materials map for Garnet, NaSICON, LiSICON, and Perovskite-type electrolytes, along with the various reported elements for substitution at different sites. Generally, the production of phase-pure solid-state electrolyte powders is referred to as synthesis. The raw components are homogenized using methods such as solid-state reaction, gel synthesis, melt quenching, microwave processing, and solution synthesis. Subsequently, high temperatures are applied to the thoroughly mixed raw materials to induce chemical reactions, leading to the breakdown of carbonate, phosphate, and other substances.

3.1. Techniques for Preparing Bulk Materials

3.1.1. Solid-State Reaction

The term “solid-state reaction approach” describes a powder sintering technique in which no melting occurs during the sintering process. One of the simplest and quickest methods to produce solid-state electrolytes is to combine the solid components directly and then sinter them to initiate their physiochemical reactions. In the literature, this type of synthesis is also known as solid-state, ceramic, or high-temperature preparation, and it is commonly used for preparing oxide SSEs. Solid-state reaction methods are typically employed to prepare garnet-type SSEs. The solid-state reaction process involves four simple stages: measuring, mixing, drying, and sintering (Figure 4a). Before starting, it is essential to verify the ratios of the initial ingredients needed to produce the desired final product.

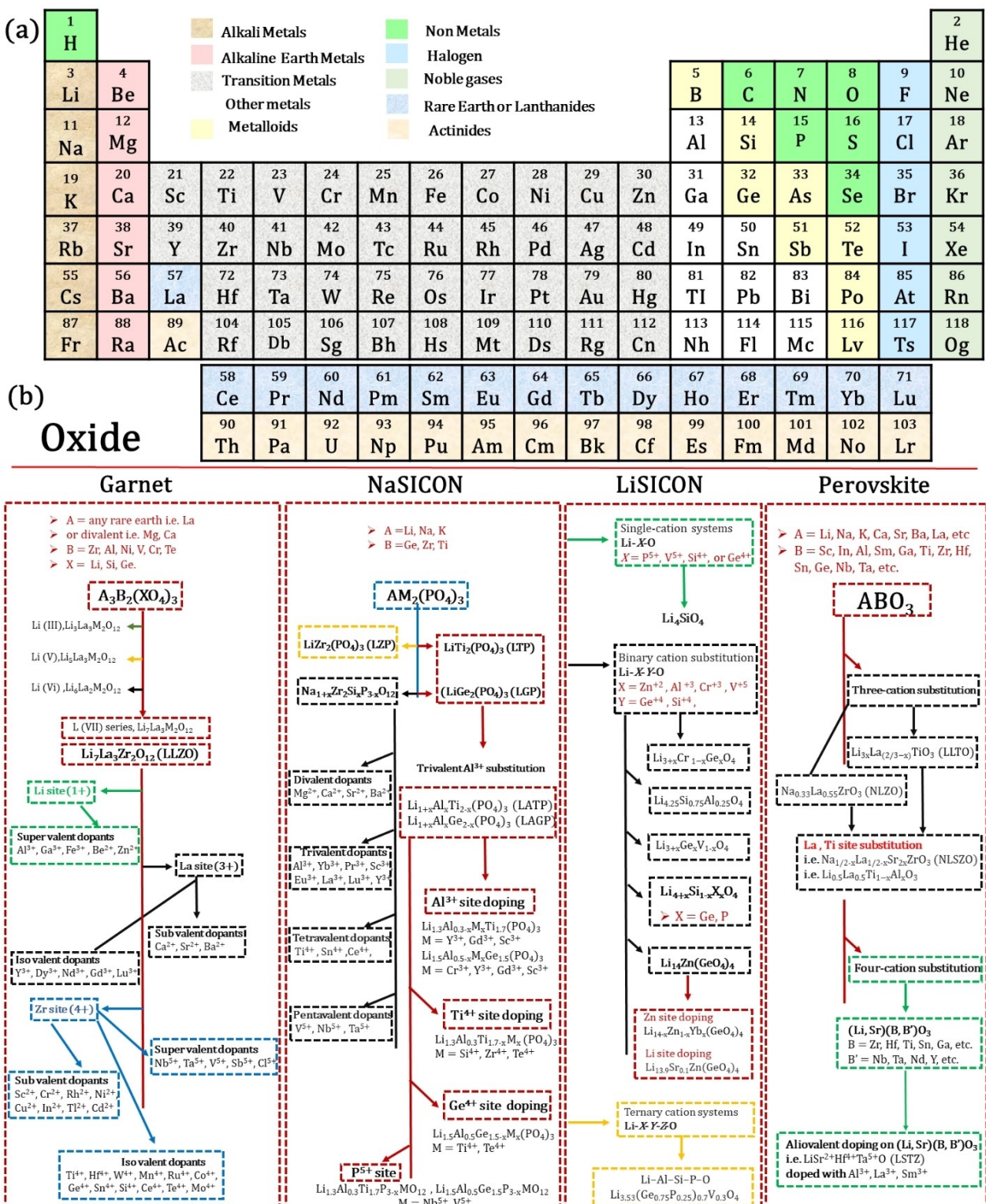


Figure 3. (a) Periodic table, (b) Materials map of Garnet, NaSICON, LiSICON, and Perovskite type electrolyte and discussed the different reported elements for substitution on different sites.

Any potential variations caused by the moisture content and quality of the precursors should be considered throughout the analysis procedure.^[9,21]

The measured raw ingredients must be thoroughly mixed, which can be done using a mortar and pestle or the ball milling approach. Manual grinding typically takes many hours to properly mix the components. The most popular and efficient

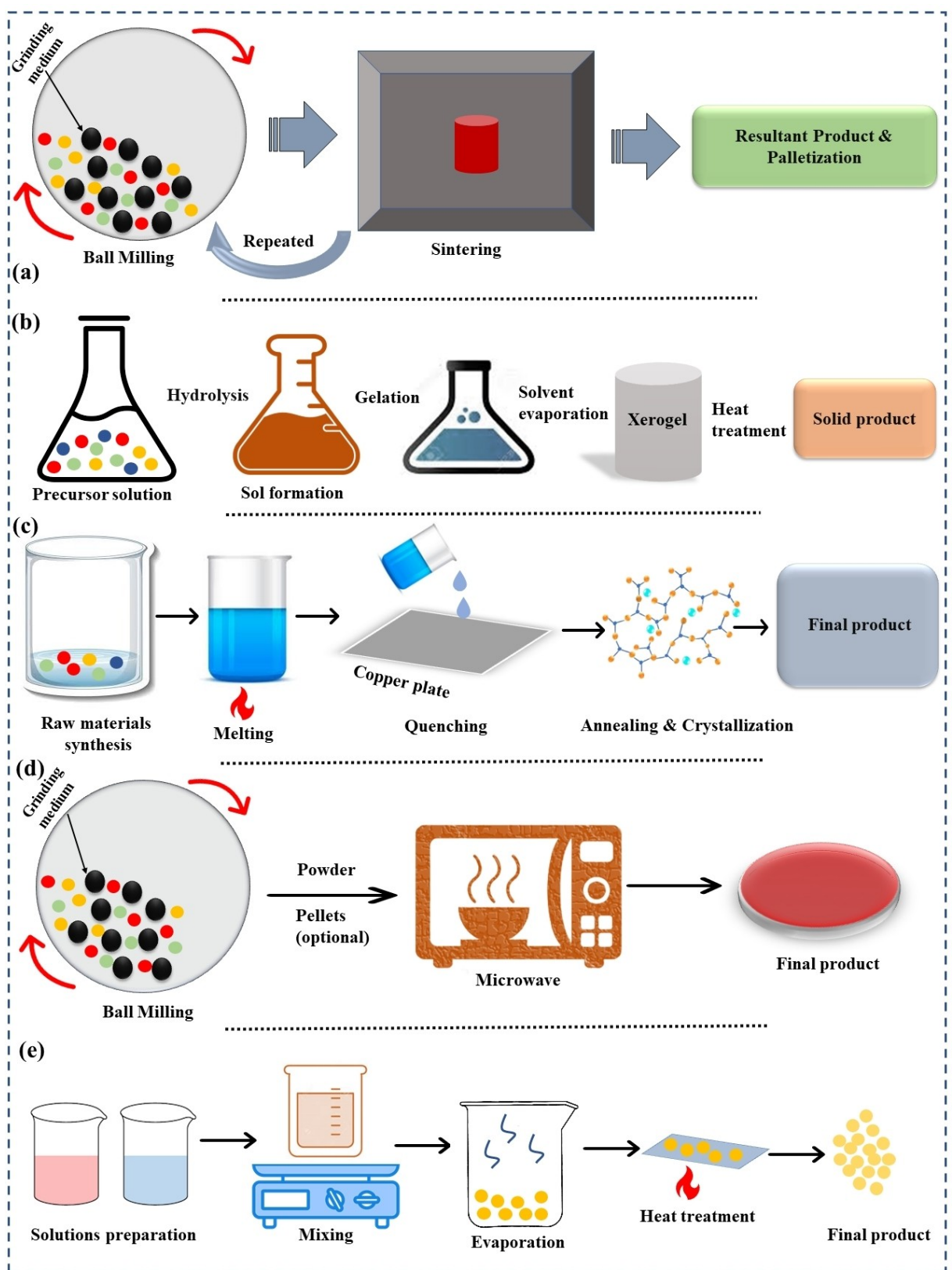


Figure 4. Schematic illustration of (a) Solid-state reaction, (b) Sol-gel synthesis, (c) Melt quenching method, (d) Microwave synthesis, and (e) Solution synthesis.

method to finely grind powder and enhance the consistency of reagent mixing is ball milling. Generally, planetary ball mills are

more effective than drum ball mills for grinding. It is important to note that high-hardness zirconium dioxide balls are

frequently used in the ball milling method, which may introduce contaminants into the starting materials. Therefore, the milling duration must be carefully monitored throughout the mixing process. The ball mill should be loaded with various-sized ball-milling pellets and ball-milling liquids. The solvents used in ball milling are believed to help reduce particle size, which generally benefits sintering due to the smaller particles. Although alcohols efficiently reduce particle size, commonly used iso-propanol solutions significantly decrease Li⁺ due to Li⁺/H⁺ exchange, hindering densification during the sintering process. This issue can be mitigated by adding a small quantity of surfactant and using acetonitrile.^[116,117]

Wet milling also helps to increase the mobility of raw materials. When selecting a liquid for ball milling, it is always preferable to use an insoluble solution because the weighted powder of the preliminary raw material should be insoluble in it. There should be specific limits on the consumption of fluids, as inadequate or excessive liquid will cause inconsistent mixing. The typical weight ratio of balls, powdered form, and liquid is 4:1:1, but it may be adjusted to fit other systems. The obtained slurry or latex paint is then placed into an uncovered container and dried completely in an oven. A strainer is used to separate the balls from the powder, which is then calcined at a high temperature. The particle size and grain boundary width of the solid-state electrolyte are influenced by time and temperature during the sintering process, which in turn affects the total conductivity of the SSE. Additionally, the possibility of lithium loss during the high-temperature sintering process must be considered, which is why a small amount of extra lithium content is frequently added during ball milling. To achieve the desired outcome using the solid-state reaction method, high temperatures, prolonged heating times, and continuous grinding are often required. Ultimately, the outcomes of solid-state preparation can be significantly impacted by these regulations. To completely rule out any potential for reagent reactions, a standardized vessel for the reaction should be selected, with common options including alumina, silica, and carbon glass. The solid-state reaction requires high temperatures ranging from 700–1200 °C and a lengthy dwell time of more than 12 hours.^[9,21,100] The solid-state reaction approach, while being a straightforward synthesis process, has some drawbacks. The high sintering temperature and prolonged heating treatment can cause Li evaporation, affecting the product architecture. Additionally, due to the volatile nature of Li at high temperatures, it is challenging to regulate the chemical equilibrium of Li garnets through solid-state production. The inhomogeneity of the final product and the appearance of impure phases are two further significant issues associated with the solid-state reaction process.^[118]

3.1.2. Sol-Gel Synthesis

Inorganic ceramic materials were first synthesized using the sol-gel method in the mid-19th century. The sol-gel approach is one of the most effective wet-chemical procedures for producing phase-pure, uniformly sized nanopowders. The concept

behind the sol-gel method is to mix the raw ingredients equally in a liquid medium, using a precursor molecule with a highly chemically reactive component. The following crucial processes are involved in the sol-gel approach: (a) hydrolysis, (b) gelation, (c) polymerization, (d) drying, and (e) dehydration (Figure 4b).^[38] Hydrolysis can be accelerated to an optimal level by gradually adding an alkaline substance to the metallic salt solution, resulting in the formation of a hydroxide sol. The stable, translucent sol that forms is due to hydrolysis and the subsequent condensation of chemical processes. Over time, the colloidal particles in the sol gradually transform into a gel with a three-dimensional framework structure. The obtained gel is then sintered, dried, and hardened to produce materials with nanostructured or micron-sized features.^[119] One effective way to mitigate the impact of metal ion variation in the sol-gel method is to include a complexing agent. A common complexing agent used for this purpose is citrate.^[9]

The sol-gel procedure involves several key steps. To create a stable sol structure without precipitation, we first select appropriate liquid chemical additives or powdered chemicals that dissolve in the liquid or sol as initial ingredients. These are then mixed and reacted evenly in the liquid state. Drying under normal pressure removes the sol liquids, causing the material to shrink and form a substance known as a xerogel. If the obtained fluid is alcohol-based, the gel is often referred to as an alcohol gel. Aerogels can be considered a type of "xerogel," while the general term "gel" typically describes either alcohol gels or xerogels. After sintering and synthesis, the desired product is recovered from the dehydrated fluid, which now exists as solid particles in the sol or gel phase.^[120] One of the key advantages of the sol-gel approach is its ability to achieve strong chemical uniformity at the nanometer scale, which can lower the operating temperature required for calcination. The purity of particles generated by the sol-gel technique is significantly influenced by the additive ingredients. In contrast, particles produced by the solid-state reaction technique might be less pure due to contamination from ball mill beads during prolonged, high-energy grinding. The sol-gel method is widely used to synthesize oxide solid-state electrolytes and offers several advantages over other techniques: (a) it allows precursors to quickly attain molecular-level uniformity because the starting materials are initially dissolved in a solvent to create a low-viscosity solution; (b) it simplifies the even and direct addition of minor elements; and (c) component dispersion in sol-gel structures is typically in the nanometer range, whereas in solid-phase processes, it is usually in the micrometer range. Additionally, the sol-gel process is simpler and requires lower synthesis temperatures compared to solid-phase methods. However, the sol-gel technique has its drawbacks, including the high cost of raw materials, the use of hazardous chemical solvents, a lengthy process, potential residuals in the desired products, and gas and organic material leakage. Factors such as the pH level of the solution and the drying environment can impact the performance of sol-gel powders. Furthermore, the sol-gel process typically produces smaller quantities and involves a more complicated preparation procedure than the solid-state reaction method. Consequently, the sol-gel process

is often not the preferred method for preparing ceramic powders.^[9,21]

3.1.3. Melt-Quenching Method

A novel class of inorganic compounds with potential applications as solid-state electrolytes is glass ceramics. These materials are prepared by heating raw ingredients to specific conditions that induce both crystalline and glassy phases, resulting in a product known as glass ceramics.^[121] Glass-ceramics are produced through a carefully controlled crystallization process in glassware. Specifically, the parent glass, with a defined composition, is heated according to a predetermined heat treatment regimen. Compared to the crystals found in pure ceramic materials, the crystallized structure within glass ceramics is notably more homogeneous, polished, denser, and virtually free of residual porosity. Traditionally, glass-ceramic materials are prepared using the melt-quenching technique. This conventional approach is also commonly used for producing NaSICON-type materials.^[100]

The preparation procedure can be outlined as follows: After thoroughly mixing the raw ingredients, they are added to a crucible and heated to a high temperature, allowing them to settle for several hours. The molten material is then rapidly quenched by pouring it onto a copper plate for swift cooling (Figure 4c). Alternatively, the material can be poured into a specially designed mold to achieve the desired form. To facilitate nucleation and crystallization, the material is subsequently annealed at a specific temperature. The annealing process helps to eliminate defects such as pores, micro-cracks, and heat stress. The temperature is then raised to the crystallization temperature, maintained there, and finally cooled to produce the glass-ceramic substance. It is important to note that the annealing process, following melting, is crucial. The annealing process controls the crystal concentration, phase forms, and grain size in the glass ceramics, resulting in materials with excellent density but requiring high preparation temperatures. Crucibles made of platinum, alumina, or rhodium-platinum can be used in the preparation process, with platinum-based crucibles recommended to prevent contamination at high temperatures. The melt-quenching approach has been successfully used to synthesize oxide-based solid-state electrolytes, such as LAGP. Generally, LAGP synthesized by the melt-quenching technique exhibits higher ionic conductivity compared to LAGP obtained through solution synthesis.^[21,122]

3.1.4. Microwave Synthesis

Microwave synthesis is a recent and emerging technique for material preparation. In contemporary society, microwave ovens are widely used as common household appliances. Microwaves, which have frequencies ranging from 300 MHz–30 GHz, are a form of non-ionizing electromagnetic energy. There are two key processes involved in microwave heating: ionic conduction for ions and dipolar polarization for dipoles. Microwaves, as high-

frequency electrical fields, are typically used to heat polar materials. When polar compounds are exposed to electromagnetic radiation, their molecules align with the microwave field, causing them to spin and collide, which releases energy. This movement generates heat through molecular friction and dielectric loss. Unlike conventional heating methods, which heat materials from the outside, microwave heating generates heat directly within the material. The schematic illustration of microwave synthesis is shown in Figure 4d. This method allows for more uniform heating of the sample and can accommodate various sizes and structures of the heated item.^[21,123]

Microwave heating offers several advantages over traditional ovens, including accelerated reaction rates, milder reaction conditions, increased chemical yields, reduced energy consumption, and enhanced reaction specificity. However, there are also some drawbacks to microwave heating. If reaction parameters are not properly controlled, there is a risk of solvent heat escape, which can occasionally lead to explosions.^[124] Oxide-based SSEs have been successfully prepared using the microwave synthesis method. Amores et al. (2016) prepared $\text{Li}_{6.5}\text{Al}_{0.25}\text{La}_{2.92}\text{Zr}_2\text{O}_{12}$ garnet material via microwave synthesis.^[125] Nowadays, because certain starting materials strongly absorb microwave energy, using microwaves in solid-state production is emerging as an alternative technique. This method can reduce both reaction times and heating temperatures.^[118]

3.1.5. Solution Synthesis

In solution synthesis, raw ingredients are typically mixed with a solvent to initiate the reaction. As the reaction progresses and becomes robust, the solvent evaporates, leaving behind a solid-state electrolyte powder, which is then prepared through heat treatment (Figure 4e). Unlike solution synthesis, the sol-gel technique involves additional steps of mixing precursors in the liquid phase to form a sol, which is a different kind of reaction. Solution synthesis generally has fewer experimental prerequisites compared to sol-gel methods. However, to produce rapid ionic conductors efficiently and reproducibly using solvent routes, careful formulation of the synthesis process is still required. The fundamental chemical pathways for generating ionic conductors via solution methods are not well understood. Moreover, solid-state electrolytes produced through solution synthesis typically exhibit lower ionic conductivity compared to those developed using the solid-state reaction technique, which usually has one order of magnitude higher ionic conductivity.^[21]

Since each synthetic method has its distinct advantages and inherent drawbacks, informed and independent judgments should be made based on a thorough understanding of the specific electrolyte systems and their requirements. Figure 5 summarizes the pros and cons of various synthesis methods for solid-state electrolytes.

Solid state reaction	Sol-gel synthesis	Melt-Quenching	Microwave synthesis	Solution synthesis
<ul style="list-style-type: none"> ✓. Simple and quick ✓. Cheap reactants ✓. Massive produce 	<ul style="list-style-type: none"> ✓. Excellent purity ✓. Cheap facility ✓. Homogeneity 	<ul style="list-style-type: none"> ✓. Glass ceramics ✓. Homogeneity 	<ul style="list-style-type: none"> ✓. Accelerated reaction Rates ✓. Reduced energy usage ✓. Distinct reaction Specificity 	<ul style="list-style-type: none"> ✓. Nano powder ✓. low temperature for Preparation ✓. Simplest
<ul style="list-style-type: none"> ✗. High temperature for synthesis ✗. Inhomogeneity 	<ul style="list-style-type: none"> ✗. Complex Mechanism ✗. Hazardous Solvents 	<ul style="list-style-type: none"> ✗. Complicated ✗. High temperature requirement 	<ul style="list-style-type: none"> ✗. Difficulty to Control ✗. Customized Setup 	<ul style="list-style-type: none"> ✗. Organic waste ✗. Poor ionic Conductivity

Figure 5. Summary of pros and cons of different synthesis methods for solid-state electrolytes.

3.1.6. Ultrafast Synthesis Method

Many traditional procedures for preparing new materials remain inefficient, as they often require high temperatures and extended periods ranging from hours to days to produce a single batch of samples. This lengthy process further diminishes the effectiveness of the research. To overcome this time-consuming challenge and accelerate the development of novel, energy-efficient, and environmentally friendly materials, there is a pressing need for new preparation and production techniques that significantly reduce labor, time, and energy consumption.

One promising advancement is ultrafast synthesis techniques, particularly ultrafast high-temperature sintering (UHS) using Joule heating. This method has gained significant interest due to its ability to synthesize various materials, from nano to bulk forms, with sample creation times often reduced to just a few seconds or less.^[126] Hu's group reported the UHS method to create a Ta-doped LLZO garnet-type ceramics pellet in a couple of seconds.^[127] Although garnet-type lithium solid-state electrolytes have been successfully synthesized using the UHS approach, however, Zuo *et al.* successfully demonstrated the creation of NASICON-type solid-state electrolytes employing the UHS technique in 2023.^[126] In 2022 Chen *et al.* established a microwave-assisted ultrafast sintered technology (MAUST) for different ceramic electrolytes using household microwaves in the atmosphere. Using graphite black as a microwave balancer, the greenish bodies hidden inside the graphite black matrix could be compressed within 25 s.^[128] In 2023 Feng *et al.* applied the UHS technique for investigating the LLZO garnet SSEs as a case study to explore the possibility of ultrafast synthesis in producing complicated structured high-entropy components

and possibly enable their accelerated exploration.^[129] These techniques are incredibly fast and efficient. Ultrafast synthesis methods typically require only a few seconds to a couple of minutes, whereas traditional processes can take several hours or even days. In addition to providing more targeted and precise energy input, ultrafast techniques minimize inevitable heat dissipation by rapidly heating, cooling, and conducting. As a result, materials synthesized using ultrafast techniques may remain in their metastable states.^[130]

3.2. Techniques for Preparing Thin Films

All-solid-state batteries that use solid electrolytes offer significant energy density due to the use of high-capacity cathodes and lithium metal anodes. However, for the same anode configuration, ceramic-based materials typically have much lower energy densities compared to liquid batteries or solid batteries that use polymeric thin-film solid electrolytes. Many oxide solid electrolytes are very rigid and brittle, which complicates the assembly of solid batteries and the production of large quantities of electrolyte sections. Additionally, oxide solid electrolytes produced through high-temperature sintering are energy-intensive and not well-suited for commercial manufacturing. To address these challenges and enable the production of thin films or flexible solid electrolytes for large-scale and cost-effective manufacturing, techniques such as sputtering with magnetron and tape-casting are discussed.

3.2.1. Tape Casting

Large-scale manufacturing of solid electrolytes is challenging with conventional methods due to constraints on energy, cost, and the ability to produce electrolytes with millimeter thickness. An alternative approach for large-scale production and reducing the thickness of electrolytes is the tape-casting method. This technique involves incorporating several additives with ceramic particles in a solvent to create a homogeneous and durable precursor. The process entails flowing the material onto a substrate, where the film is formed by the movement of the substrate and a scraper, with the thickness controlled by the gap between them. The film is then transferred to a drying chamber. During solvent evaporation, ceramic particles are bonded together by a binder, resulting in a thin sheet with specific durability and flexibility. The dried thin sheet, along with the substrate, is then cut or shaped as needed before being sintered to produce the final product (Figure 6).^[9,131]

3.2.2. Magnetron Sputtering

Magnetron sputtering is a type of physical vapor deposition that offers several advantages, including precise control, strong adhesion, extensive coating area, and relatively simple equipment. Initially used for creating metals, electronic components, insulators, and various other materials, this method is now being explored for the production of solid electrolyte thin films for SSLBs and for investigating doped thin films. The goal is to produce a solid electrolyte with high purity. By placing the material on a substrate and adjusting the sputtering power and temperature in an inert atmosphere, an optimal electrolyte layer can be achieved. In 2016, Lobe et al. investigated the effect of deposition temperature on the production of Li₇La₃Zr₂O₁₂ thin films.^[132] These methods produce thin-film

oxide solid electrolytes with satisfactory quality while minimizing lithium degradation during the film deposition process using magnetron sputtering.^[9]

4. Key Parameters Affecting the Ionic Conductivity

Solid electrolyte ionic conductivity is a crucial factor in determining their electrochemical efficiency. Significant efforts have been conducted to improve SSEs ionic conductivity. To learn about the mechanisms and parameters that affect the ionic conductivity in SSEs, we will present pertinent research on three factors that affect ionic conductivity.

4.1. Structure

The mechanics and conductivity of ionic transport can vary significantly depending on the crystal structure. There are notable differences between ion conduction processes in liquid and solid-state electrolytes. In liquid electrolytes, lithium-ion transport involves the movement of dissolved Li ions through a solvent medium. The ionic conductivity in liquid electrolytes can be enhanced by increasing the dissociation of salts/ions in solvents with higher dielectric constants and by reducing viscosity, which facilitates the movement of solvated ions. The potential energy landscape for mobile Li ions in liquid electrolytes is relatively flat due to the homogeneous environment and the rapid interchange among solvent and solute molecules.^[133] In contrast, solid-state electrolytes feature periodic bottleneck sites that form effective barriers, which mobile species must cross to diffuse. The energy required to overcome these barriers, known as migration energy, significantly influen-

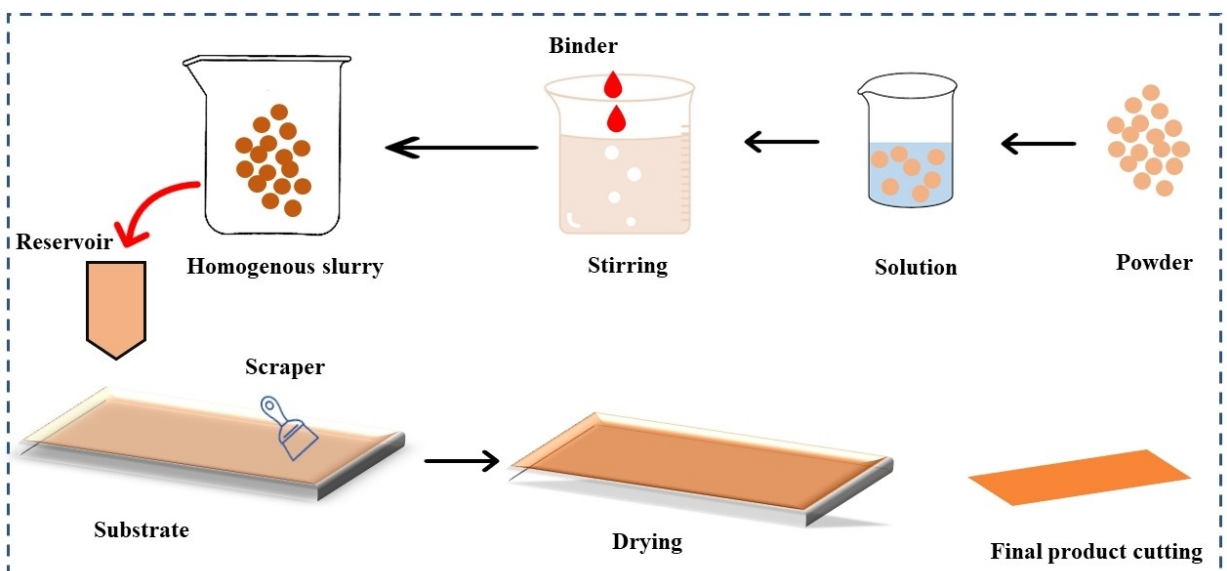


Figure 6. Schematic illustration of Tape casting.

ces ionic movement and conductivity. Lower migration energy leads to higher ionic mobility and conductivity.^[134,135] There is a significant correlation between crystal structural defects and ionic conductivity. In inorganic solid electrolytes, Li-ion movement is highly influenced by defects. These defects can take various forms, including planar defects, electronic defects, volume defects, and point or line defects. Among these, point defects have the greatest impact on ion movement within crystals. Common examples of point defects include Frenkel and Schottky defects. Schottky defects involve vacancies of both anions and cations, while Frenkel defects consist of an ion displaced to an interstitial site.^[35]

The diffusion model defines ionic transport as the hopping of individual ions from one lattice point to another through diffusion pathways within the crystal structure. The energy landscape of ion movement is shaped by the crystal environment. An ion migrates over this energy landscape, and the energy barrier that impedes ionic diffusion is determined by the highest energy point along the diffusion path. To achieve significant ionic conductivity, both low activation energy and a high concentration of mobile ions are required. While the migration energy barrier and the energy landscape barrier are the same for single-ion movement, strong ion-ion interactions and a unique mobile ion structure in superionic conductors result in a reduced energy barrier for the coordinated movement of multiple ions (see Figure 7a).^[136]

Li-ion transportation is a crucial step in the overall charge-transfer mechanism within the crystals of inorganic solid electrolytes. In superionic inorganic solid electrolytes, Li-ion

transport is governed by three factors: the type of carrier, the type of diffusion channel, and the nature of the diffusion process. The type of carrier and defect chemistry are closely related, while the diffusion route and anion arrangement are highly interconnected. In 2015, Wang et al.^[137] discussed that the anion packing of the body-centered cubic exhibits lower activation hurdles than face-centered cubic, and hexagonal close-packed and makes it capable of optimal ion flow rates. Inorganic solid-state electrolytes generally exhibit three lithium diffusion types or mechanisms. i) vacant direct hopping, ii) interstitial knock-off, and iii) interstitial straight hopping (Figure 7b) which influences the ionic conductivity.^[138] In general, crystalline solids ion conductivity follows the Arrhenius equation. However, in formations without long-range sequences, the ion conductivity deviates from the basic Arrhenius law and is best described by the Williams Landel Ferry equation.^[139] Defect sites could have minimal impact on one another in crystallized inorganic solid electrolytes, but in amorphous structures with numerous defects, it is important to analyze the connection between the movement of ions and the relationship between Li⁺ and structural ions.^[140] Additionally, no clear theories explaining ion diffusion behavior in disordered systems have been established to date. However, experiments have shown that some amorphous SSEs exhibit higher ionic conductivity compared to their crystalline counterparts. This enhancement is likely due to the extensive defects present in the amorphous materials. Furthermore, studies suggest that combining crystalline compounds with amorphous materials can improve conductivity, potentially due to the larger defects surrounding

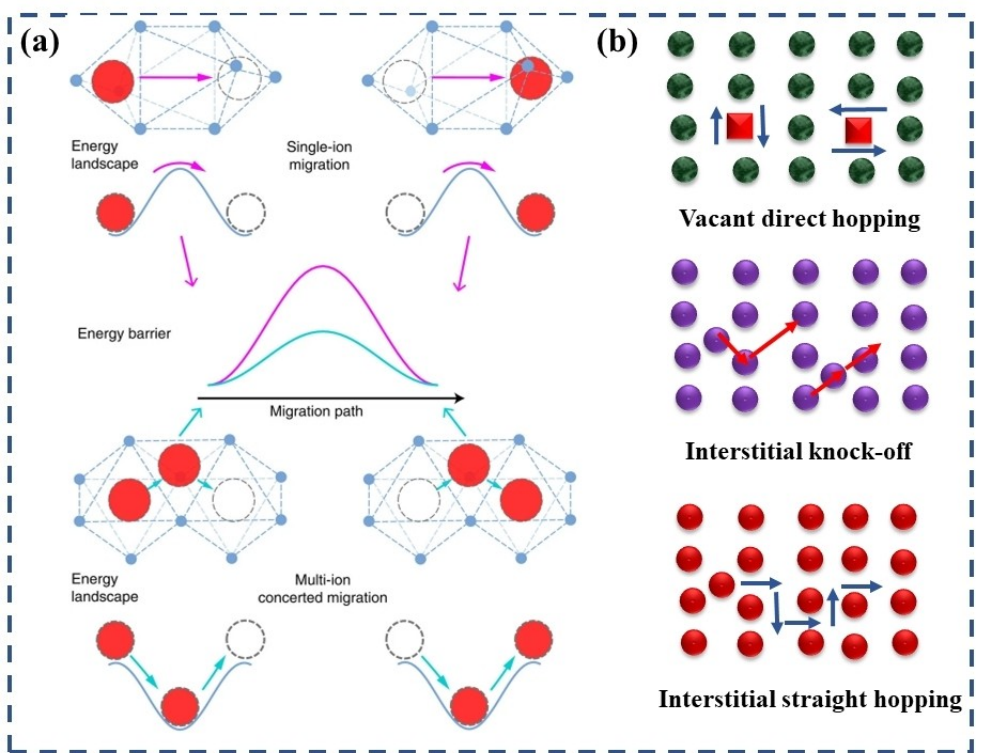


Figure 7. (a) Schematic illustration for single-ion migration vs multi-ion migration. Reprinted with the permission of.^[136] Copyright © 2017, Springer Nature. (b) Lithium diffusion mechanisms.

the crystalline regions.^[141] The amorphous and crystallographic materials could permit ion transport through multiple paths, and the arrangement and distribution of distinct stages could render the process considerably more practical. Multiphase compositions can enhance the intricate nature of the ion transportation process.^[142] Novel FCC-packed oxide solid electrolytes exhibit the objective of improving ionic transport by lowering migration energy constraints. FCC arrangements are used by materials like Li-rich compounds to provide high-density ion transportation channels with conductivities that are approximately 10^{-4} – 10^{-3} S/cm. These FCC architectures improve conductivity and durability under operating pressures by optimizing site allocation for lithium ions. These frameworks strong coordination facilitates effective lithium-ion movement, which makes them suitable for long-cyclic solid-state batteries.^[143]

As we above mentioned, it is crucial and challenging to build a stable and effective charge transport channel in solid-state batteries. Mixed Ionic Oxide Conductors (MIOC) with inherent qualities especially their capacity to transport ions and electrons simultaneously, mechanical adaptability, and structural designability, have made them a possible substitute for traditional conductors to address challenges. The dual functionality of MIOC solves the basic problem of charge transport failure and interface resistance in SSB cathodes.^[144] In addition to the cathode side, the anode side faces several charge transport limiting issues, such as volume fluctuation, mismatched charge distribution, interface instability, and unregulated Li dendritic development. Remarkably, MIOC has been investigated as a possible tactic to deal with the interface problems related to the Li metal anode in SSBs. Due to their exceptional electrical conductivity, MIOC uniformly distributes the potential throughout the surface of the Li metal. By lowering the overpotential needed for lithium deposition, this balanced potential dispersion lessens the probability that lithium dendrites will develop.^[145] Recent developments in MIOC demonstrate that mixed-cation frameworks significantly increase lithium-ion transport.^[143]

Additionally, promotes constant diffusion of Li between grain boundaries by carefully adding dopants such as Ta, Al, and Ga which assist in stabilizing the cubic phase and reducing restrictions to Li migration. In LLZO, Li atoms sporadically and partially fill the gaps in the overall structure, composed of 6-fold linked ZrO₆ octahedra and 8-fold linked LaO₈ dodecahedra. A possible explanation for the 48 g–96 h site distance is the Li⁺-Li⁺ repellent forces between shared sites face and nearby four octahedral enclosures share the tetrahedral cage sides, forming a 3-dimensional network of conduction routes.^[26,146] It is possible to significantly increase the ionic conductivity of cubic LLZO-type SSEs by developing lithium-ion vacancies using the substitution of elements such as Ta, Al, Ga, Nb, Sb, W, and Te.^[25,147] Modifications in the Li-ion arrangement in both sites (octahedral and tetrahedral) of the garnet structure by employing the aliovalent replacement of Ba or another element with La and the aliovalent replacement of Zr by Sb, Ta, or Nb can additionally lead to an increased in Li-ion conductivity.^[61,78] Discovering a stable dopant species and a way to lower LLZO

intrinsic resistance is crucial. Applying basic principles, Miara et al. estimated all potential doping elements and location preferences in LLZO. The doping at the Li, La, and Zr sites may give an outcome with strong ionic conductivity.^[148] Jin & McGinn reported that aluminum-doping may stabilize the cubic form of Li_{6.25}La₃Zr₂Al_xO₁₂ and the ionic conductivity of Al-doped LLZO is 0.2 mS cm⁻¹.^[149] Li et al. reported that room temperature Li⁺ ion conductivity of prepared Li_{7-x}La₃Zr_{2-x}Ta_xO₁₂ is 1 mS cm⁻¹.^[42] Deviannapoorani et al. reported that the Li-ion conductivity of Te-substituted Li₇La₃Zr₂O₁₂ cubic garnet material is 1.02 mS cm⁻¹.^[43] The Li_{6.55+y}Ga_{0.15}La₃Zr_{2-y}Sc_yO₁₂ was synthesized by Buannic et al. employing the double substitution technique, the addition of Sc might lead to a rise in Li-ion numbers, whereas the substitution of Ga could stabilize the cubic crystal structure of material exhibited the maximum ionic conductivity (1.8 mS cm⁻¹) at 27 °C.^[44] The Li_{6.55}Ga_{0.15}La₃Zr₂O₁₂ was synthesized by Qin et al. and showed the Li⁺ ion conductivity of 2.06 mS cm⁻¹ at room temperature.^[45] Abrha et al. effectively created a solid-state garnet electrolyte with the substitution of Ga and Nb (Li_{6.05}La₃Ga_{0.3}Zr_{1.95}Nb_{0.05}O₁₂) using the sol-gel process, it significantly enhanced its ionic conductivity (9.28 mS cm⁻¹ at room temperature) achieving the highest number recorded to date.^[46] The LLZNb (Li_{7-x}La₃Zr_{2-x}Nb_xO₁₂) as well as LLZ-Ta (Li_{7-x}La₃Zr_{2-x}Ta_xO₁₂) garnet-type oxide materials where Nb and Ta have been substituted for Zr site in LLZO are highly desirable due to their wide lithium-ion conductivity.^[81,150,151] The sintering additives could be used to enhance the pellet densities and reduce the total number of grain boundaries and sintering temperature, resulting in another method of increasing ionic conductivity in LLZO solid electrolytes. The LBO (Li₃BO₃) has been investigated as a sintering additive for LLZO solid electrolytes to boost LLZO conductivity at temperatures smaller than the normal sintering temperatures for LLZO solid electrolytes.^[88,152] In the perovskite crystal structure, Corner B sites are occupied by Ti-ions, whereas Li and La ions hold center A sites. When migrating from one location to another, Li-ions might run into difficulties when oxygen-ions create blockages. Many efforts have been made to increase the perovskites lattice constants since achieving so may modify the size of the barriers. In 1994 Inaguma et al. obtained bulk ionic conductivity of 1.5 mS cm⁻¹ by doping Li_{1/2}La_{1/2}TiO₃ with Sr²⁺. The Sr substitution for La and Li raised the perovskite structure lattice parameters.^[153,154]

4.2. Composition

Early research primarily focused on the bulk characteristics of ion transport mechanisms. However, it soon became evident that boundary layers significantly impact ion conductivity properties and are fundamentally interconnected. Ionic conductivity is just one aspect of material performance, which is greatly influenced by its composition. The conductivity of solid-state electrolytes depends on the types of ions present and their relative concentrations. Higher ionic conductivity is typically associated with greater concentrations of mobile ions. The ion transport system and the availability of charge carriers

are determined by the material's stoichiometry and chemical composition. Generally, the ionic conductivity of garnets incorporating lithium commonly rises with increasing lithium content throughout a broad range of Li percent.^[75] More precisely, the alteration in lithium-ion conductance from the Li (III) to Li (VII) series supports the idea that greater lithium concentrations are favorable for increased Li-ion conductivity. The strategy to raise NaSICON ionic conductivity may be as follows: (i) Raising Na ion concentration in the structure lattices. A higher amount of sodium ions indicates a greater quantity of charge transporters, which is advantageous for improving ionic conductivity. (ii) The activating energy and energy restriction for the movement of Na ions may be lowered by increasing the bottle-neck size by adding appropriate substitutes. (iii) Enhancing Na ion conductivity at grain boundaries and reducing resistance at those points. Compared to the ion transport within the grain bulk, the movement of ions across the grain bordering is considerably more intricate.^[155] The bottleneck size and site percolating are the two parameters that control the conductivity of NaSICON type SSE.^[24] The improved interface effects and synergistic interactions contribute to the enhanced ionic conductivity of SSEs. For instance, the ionic conductivity of the double-phase $\text{Li}_1\text{Al}_2\text{O}_3$ is notably higher than that of the single-phase materials.^[156]

Compression alteration can optimize the ionic conductivity of solid-state electrolytes by selecting an appropriate aliovalent dopant and achieving the ideal doping concentration. Doping can be either homogeneous, resulting in a solid solution, or heterogeneous, creating a composite material. In inhomogeneous doping, the introduction of aliovalent cations generates oxygen vacancies. These vacancies serve as a conduit for the conduction of oxygen ions. Regarding zirconia-based networks, Sc^{3+} surpasses Ca^{2+} , Y^{3+} , and so on in terms of creating an open channel for conduction, while Mg^{2+} is a less active dopant.^[157] Multiple doping approaches often promise more significant improvements in the ionic conductivity of SSEs compared to single doping. These enhancements are typically based on the chemical composition and phase structure of the material. However, in some cases, ionic conductivity may decrease. This reduction is not always due to the characteristics of the dopants themselves but can result from the improved segregation of impurities at the grain boundaries. Another method for enhancing ionic conductivity is to use heterogeneous dopants that are only partially soluble in the bulk structure of materials such as zirconia.^[158] In the $\text{Na}_3\text{Zr}_2\text{Si}_2\text{PO}_{12}$ structure, at the Zr^{4+} site, hetero-valent or iso-valent substitution significantly boosted the conductivity. Song et al.^[50] have conducted a thorough study on the effects of divalent dopants, such as (Mg^{2+} , Ca^{2+} , Sr^{2+} , and Ba^{2+}). Interestingly Mg^{2+} doping leads to the greatest conductivity of 3.5 mS cm^{-1} at room temperature. Lu et al. reported that 5% Ca^{2+} substitution on NaSICON raised its ionic conductivity to 1.67 mS cm^{-1} .^[51] Similarly, Al doping on $\text{Na}_3\text{Zr}_2\text{Si}_2\text{PO}_{12}$ ($\text{Na}_{3.55}\text{Zr}_{1.85}\text{Al}_{0.15}\text{Si}_{2.40}\text{P}_{0.60}\text{O}_{12}$) composition demonstrates total ionic conductivity of 2.1 mS cm^{-1} at room temperature.^[53] Researchers also looked at the impacts of trivalent ions, such as (Yb^{3+} , Pr^{3+} , Sc^{3+} , Eu^{3+} , Lu^{3+} , and Y^{3+}), from these Sc^{3+} is one of the best substituents

for $\text{Na}_3\text{Zr}_2(\text{SiO}_4)_2(\text{PO}_4)$ since Zr^{4+} and Sc^{3+} exhibits closest (0.72 \AA) and (0.745 \AA) ionic radii respectively. These Sc-doped materials attain notably high ionic conductivities up to 4 mS cm^{-1} . By adding Nb^{5+} at the Zr^{4+} of site $\text{Na}_{3.4}\text{Zr}_2\text{Si}_{2.4}\text{P}_{0.6}\text{O}_{12}$, the impact of pentavalent substitution was depicted. As the amount of Nb rises, there is a propensity for the ionic conductivity to first rise and subsequently decrease. The obtained ionic conductivity for $\text{Na}_{3.3}\text{Zr}_{1.9}\text{Nb}_{0.1}\text{Si}_{2.4}\text{P}_{0.6}\text{O}_{12}$ is 5.5 mS cm^{-1} .^[97] The high interstice lithium ion concentration enhances the ionic conductivity.^[60,154] A further helpful approach for enhancing ionic conductivity in LISION solid electrolytes is substituting Cl^{1-} for O^{2-} . The LiSICON solid electrolytes ($\text{Li}_{10.42}\text{Si}_{1.5}\text{P}_{1.5}\text{Cl}_{0.08}\text{O}_{11.92}$) and ($\text{Li}_{10.42}\text{Ge}_{1.5}\text{P}_{1.5}\text{Cl}_{0.08}\text{O}_{11.92}$) having ionic conductivities of $1.03 \times 10^{-2} \text{ mS cm S cm}^{-1}$ and $3.7 \times 10^{-2} \text{ mS cm}^{-1}$ at 27°C respectively, were synthesized by Song et al. (2015) via partially doping O^{2-} with Cl^{1-} . The partial replacement may result in larger bottlenecks and higher lattice parameters for Li-ion transport. In addition, there is less bonding b/w Li^+ and Cl^- than Li^+ and O^{2-} due to lower electronegativity. The Cl-doped LiSICON electrolytes possessed high ionic conductivities as a consequence of all of these effects.^[64,154] Generating anions at Si sites might dramatically enhance the $\text{Li}_{4+x}\text{Si}_{1-x}\text{X}_x\text{O}_4$ ($\text{X}=\text{Ge}, \text{Al}$ or P) group's ionic conductivity at room temperature by numerous orders of magnitude. Deng et al. (2017) utilized simulations and performed tests to study $\text{Li}_{3.75}\text{Si}_{0.75}\text{P}_{0.25}\text{O}_4$, $\text{Li}_{4.25}\text{Si}_{0.75}\text{Al}_{0.25}\text{O}_4$, and $\text{Li}_4\text{Al}_{0.33}\text{Si}_{0.33}\text{P}_{0.33}\text{O}_4$. A hybrid polyanion impact which lowers the temperature of transitioning between diffusion processes and increases ionic conductivity could arise from substituting Si in Li_4SiO_4 with Al, P, or Ge. The ionic conductivity $9 \times 10^{-1} \text{ S cm}^{-1}$ is significantly greater than Li_4SiO_4 at ambient temperature.^[66] In perovskite materials composition Sr expanded the Li-ion's diffusion region and enhanced ionic conductivity but when the Sr quantity exceeded 0.1 resulting a reduction in Li-ion content and ionic conductivity.^[153,154]

4.3. Dimension

A material's ionic conductivity is influenced by its dimensional characteristics, including thickness, grain size, and particle size. For example, materials at the nanometer scale may exhibit different conductivity characteristics compared to their bulk counterparts due to size-dependent phenomena. Interfaces, which are disruptions in the structural framework, often emerge alongside changes in the number of charge carriers. Additionally, reducing particle or dimension sizes can increase the interfacial area. Nanosized SSEs have significantly larger interfacial regions compared to bulk materials, leading to greatly improved ionic conductivity. Investigation on the impact of Al_2O_3 pore diameters in electrolyte composition to enhance ion conductivity was done by Maekawa et al.^[159,160] They found that decreasing particle size can significantly increase conductivity by an order of 10–50. Overall, nanocrystallization has significantly enhanced the ionic conductivity of solid-state electrolytes by creating extensive surface areas. Materials with larger surface area-to-volume ratios provide more active sites for ion transport. By increasing the surface area, the contact between

the electrolyte and electrode improves, which facilitates ion diffusion and boosts conductivity.^[3]

In LLTO, the lower total ionic conductivity is caused by LLTO grain-boundary ionic conductivity, which was merely in the range of 10^{-2} mS cm⁻¹ at ambient temperature although having a high bulk ionic conductivity.^[153,154] The existence of diverse grain boundary dimensions might impact the ionic behavior of the electrolyte composition. When the Li_{0.33}La_{0.56}TiO₃ perovskites are created at extreme temperatures, they could contribute significantly to the degradation of lithium ions in LIBs. The diverse boundaries of grains are due to the reduction of lithium ions. The CaTiO₃ is utilized to produce a thin layer on the polyethylene divider to prevent the production of dendrites. This improves the system cycle efficiency and thermal endurance.^[104]

5. Stability Complications in Solid-State Batteries

Effective battery development and manufacturing rely heavily on solid-state electrolytes and their ability to maintain proper contact with electrodes, preserving their composition and structure throughout the cycling process. A strong solid interface can form between the electrolyte and electrodes, leading to slow ion diffusion. Additionally, any vacuum or gaps between the electrodes and electrolyte can cause battery malfunctions or prevent proper cycling. The requirements for SSE synthesis and handling are influenced by factors such as the stability of the SSE against humidity, which affects battery capacity during storage due to chemical instability at the electrolyte/electrode interfaces. Thermal stability and mechanical degradation can also increase interfacial barriers, reduce ionic conductivity, and limit the overall efficiency of electrochemical devices.^[14]

5.1. Chemical Stabilization

The production and storage requirements for SSEs are largely dictated by their chemical stability. However, exposure to ambient air can lead to deterioration of certain SSEs, with some degradation products potentially posing risks to their continued use. Li⁺/H⁺ transfer, a well-documented phenomenon, has been extensively reported in oxide lithium-ion conductors.^[161] When the garnet-type LLZO SSE was first discovered, it was generally considered air-stable. However, Cheng et al. (2014) found that after just two months of exposure to air, a significant layer of Li₂CO₃ developed on the surface of the LLZO pellets.^[162] Several studies have shown that garnet-type SSEs readily react with CO₂ and H₂O from the atmosphere to produce LiOH and Li₂CO₃. This indicates that similar reactions also occur at the grain boundaries of garnet pellets.^[16] The mechanism of Li₂CO₃ production on the surface of garnet LLZO in air is illustrated in Figure 8a. Li⁺/H⁺ interchange between H₂O vapor and the garnet pellets produces LiOH·H₂O, which then reacts with CO₂ to form Li₂CO₃. This process occurs when the pellets are

exposed to ambient air.^[163] Consequently, the authors hypothesized that the significant interfacial resistance between LLZO and lithium was due to surface contaminants resulting from LLZO's chemically unstable state. In 2017, Sharifi et al. found that high interfacial resistance and poor wettability were attributed to these surface pollutants. They demonstrated that removing surface contaminants through a combination of basic wet scrubbing and thermal treatment could significantly enhance Li wettability and interfacial conductance.^[164] According to Jin and McGinn, exposure of LLZO pellets to humidity impacts both their mechanical strength and conductive properties. This effect may be attributed to the preferential reaction activities at the grain boundaries of the pellets.^[165] Oxide solid electrolytes, such as LATP, LLTO, and LLZO, generally exhibit better air stability compared to sulfide electrolytes. Specifically, LATP and LLTO demonstrate significant stability when exposed to moisture and CO₂, offering substantial advantages for battery processing and production. However, LLZO tends to form a carbon-based layer on its surface when exposed to air, which increases interfacial resistance during processing and operation.^[14] Interestingly, NaSICON electrolytes show slow deterioration in H₂O and LiNO₃ aqueous solutions. Compared to other solid-state electrolytes, NaSICON exhibits superior chemical stability in ambient conditions. The relative chemical stability of various solid-state electrolytes can be ranked as follows: Sulfide < Perovskite < Garnet < Polymer < NaSICON. The kinetic parameters also affect the ion transfer behaviors of oxide conductors. Generally, higher temperatures are associated with faster Li⁺/H⁺ exchange rates. Additionally, reaction rates are influenced by humidity. In a dry atmosphere with approximately 0.5% humidity, LLZO pellets showed less Li₂CO₃ formation compared to those in normal air with around 50% humidity. LLZO stored in dry air exhibited significantly reduced Li/LLZO interfacial resistivity. Besides humidity, the pH level of the water-based medium also impacts the ion exchange mechanism.^[10]

In addition to environmental factors, the microstructure and elemental composition of materials significantly influence ion movement. Smaller particle sizes generally correspond to higher rates of ion exchange and faster response times. It has been observed that as the tightness of Li atom bonds increases, the Li inclusion voltage also rises, contributing to greater stability. This observation might account for the differences in chemical stability against moisture. Specifically, weak Li–M bonds, which often result in high Li⁺ ion conductivity, can lead to reduced stability when exposed to moisture.^[166] Additives are an effective way to prevent undesirable reactions in the surrounding air. According to Li et al. (2017), adding 2% LiF inhibits the production of Li₂CO₃ on the LZO surface, and 2% LiF-LLZO shows less interfacial resistance with lithium metal.^[167] Another effective strategy for enhancing chemical stability involves modifying the material's chemical composition. Different oxide conductors exhibit varying ionic exchange behaviors, and therefore, optimizing the elemental composition of these oxides can be a promising approach to improve the material's chemical durability.^[168] According to calculations, the sequence of chemical stability vs moisture is Li₂La₃Sn₂O₁₂ is superior to

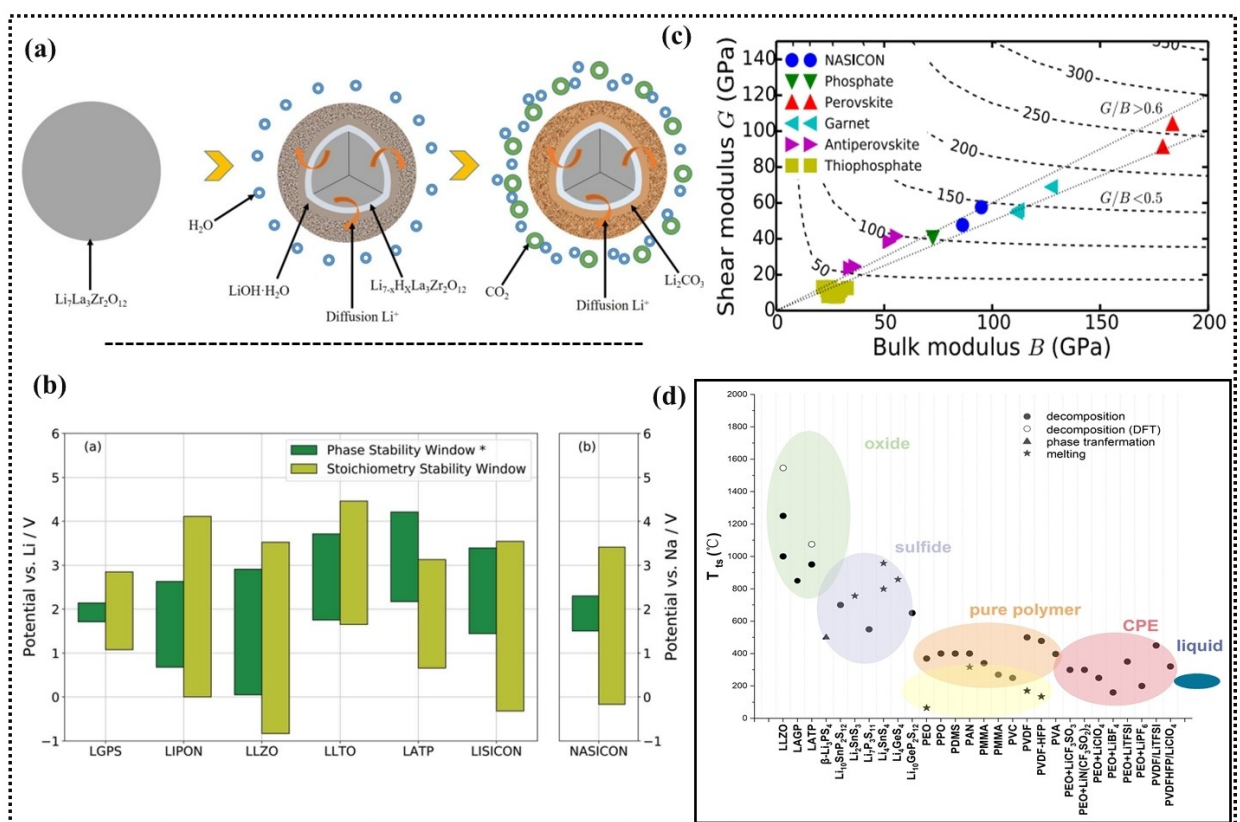


Figure 8. (a) The mechanism of Li_2CO_3 production on the garnet LLZO surface in air. Reprinted with the permission of.^[163] Copyright © 2017, The American Ceramic Society. (b) The phase stability and stoichiometry stability voltage windows for different Li-solid-state materials. Reprinted with the permission of.^[175] Copyright © 2020, Royal Society of Chemistry. (c) Shear modulus and bulk modulus measurements for different solid-state electrolytes. Reprinted with the permission of.^[177] Copyright © 2015, The Electrochemical Society. (d) Decomposition temperatures for traditional liquid and solid-state electrolytes. Reprinted with the permission of.^[178] Copyright © 2021, John Wiley and Sons.

$\text{LiLa}_3\text{Hf}_2\text{O}_{12}$ and $\text{LiLa}_3\text{Zr}_2\text{O}_{12}$. Since changes in composition and the addition of additives often lead to reductions in ionic conductivity, post-synthesis treatments of solid-state electrolytes can be effective and economical methods to produce impurity-free SSEs, especially for oxides. High-temperature treatment is used to remove surface Li_2CO_3 and improve the material's performance. In 2018 Wu et al.^[169] observed that heating the garnet pellets at 900 °C can result in stable Li-LLZO and Li_2CO_3 layer-free garnet pellets. It is crucial to carefully select the temperature for post-synthesis treatments, as excessive heat can lead to lithium loss and reduced ionic conductivity, whereas insufficient calcination may leave residual Li_2CO_3 on the surface.

5.2. Electrochemical Stability

In addition to high ionic conductivity, excellent electrochemical stability is crucial for the commercial viability of solid electrolytes. To assess the electrochemical stability of a solid-state electrolyte, several factors must be considered: (i) the predetermined potential range, (ii) chemical compatibility between electrodes and electrolyte, and (iii) the electrochemical stability of the electrolyte/electrode interface. These factors are critical

to battery performance, as the primary elements of a battery operate based on varying chemical potentials under applied voltage. Electrochemical stability, or the voltage stability window, refers to the range of voltages within which the solid electrolyte remains stable. Outside this range, the material may begin to either incorporate or release lithium ions, affecting its overall stability.^[14,170,171] For batteries with high energy densities, a wide working voltage range is preferred, necessitating that solid electrolytes remain stable over a broad voltage span. It is important to highlight that while the electrochemical stability window is a critical property of the solid electrolyte itself, it also significantly impacts interface stability. The solid electrolyte often undergoes electrochemical breakdown at the interface with the electron source, particularly when exposed to the applied voltage. Therefore, maintaining a robust electrochemical stability window is essential not only for the electrolyte's inherent stability but also for ensuring stable performance at the interface.^[37]

It is advantageous to pair a Li-metal anode and cathode with an optimally chemically stable SSE that has a voltage stability range of 0.5–5 V. This configuration minimizes parasitic reactions during battery operation. An interphase layer that forms due to the limited electrochemical stability window of the SSE can compromise the integrity of the interface between

the electrode and the electrolyte, significantly increasing interfacial resistance. Consequently, solid-state batteries may experience reduced capacity and poorer cycle performance due to diminished coulombic efficiency. However, the interphase layer can also enhance electrochemical stability if it consists of lithium binary breakdown products from the SSE, such as Li_4GeS_4 , $\text{Li}_7\text{P}_2\text{S}_8$, or $\text{Li}_6\text{PS}_5\text{Cl}$. These materials are excellent electronic insulators and ionic conductors and exhibit thermodynamic resistance against Li metal, potentially extending the battery's operational lifespan.^[14,148,172-174]

The oxidation potentials for various oxides, such as LAGP/LATP (≈ 4.2 V), LLTO (≈ 3.7 V), and LLZO (≈ 2.9 V), exceed 3 V. This is associated with the evolution of oxygen gas at high oxidation potentials and significant overpotentials due to insufficient kinetics. Overall, oxides exhibit better oxidation stability compared to sulfides.^[170,172,175] Due to their significant oxidation potential, solid-state electrolytes such as LATP and LLTO demonstrate the highest electrochemical stability with cathode materials like LCO. The electrochemical stability range for LATP varies according to different studies. The stoichiometry stabilization approach suggests that LATP is stable within a voltage range of 0.66–3.13 V. In contrast, the phase stability technique reports a wider stability range of 2.2–4.3 V. Despite numerous experimental investigations, this discrepancy remains unresolved. Figure 8b illustrates the phase stability and stoichiometry stability voltage windows for various Li-solid-state materials. Most oxide breakdown products are insulating and Li-deficient, contributing to the stability and desirable characteristics of the protective layer.^[14,170,175,176]

In addition to possessing a Li-ion exchange ratio of unity and strong ionic conductivity at ambient temperature, LLZO also exhibits outstanding stability towards Li metal. Both experimental and theoretical evidence reveals that LLZO has one of the smallest reduction potentials (0.05 V vs Li^+/Li), resulting in an extremely low thermodynamic driving force and superior resistance to reduction by lithium at 0 V. According to first-principles computation, the electrochemical stability range of LLZO is between 0.05 V and 2.91 V, which is significantly narrower than the empirically observed window of approximately 0–6 V. Han et al. (2016) reported that the oxidation breakdown of LLZO produces $\text{Li}_6\text{Zr}_2\text{O}_7$, Li_2O_2 , and La_2O_3 , which can occur at voltages as low as 2.91 V. When the voltage exceeds 3.3 V, further oxidation of Li_2O_2 generates O_2 . The reduction and oxidation of the solid electrolyte at both the anode and cathode sides create a surface passivation layer that prevents further decomposition of the electrolyte, contributing to the experimentally observed enhanced electrochemical stability of LLZO.^[14,16,172] The Li_2CO_3 inactivation layer affects the assessment of the electrochemical window. Pristine garnet-type solid-state electrolytes without Li_2CO_3 exhibit electrochemical stability greater than 4.4 V. Therefore, it is important to consider the interfacial barrier created by the breakdown of garnet-type electrolytes and the Li_2CO_3 layer.^[179] The broader electrochemical window could result from a higher overpotential caused by the sluggish kinetics of the breakdown process. It has been observed that the dopant content, crystal structure, and

chemical composition of Li oxides influence their electrochemical stability.

5.3. Mechanical Steadiness

Identifying the mechanical characteristics of solid electrolytes has become increasingly important, as these properties are crucial for the construction and manufacturing of solid-state battery designs with enhanced electrochemical efficiency.^[180] The mechanical characteristics of solid electrolytes can be classified into three categories: elastic, plasticity, and fracturing characteristics. The shear modulus is defined as the ratio of shear stress to shear strain and can be calculated using the formula $E=2G(1+\nu)$, where ν represents Poisson's ratio, E denotes Young's modulus, and G stands for shear modulus. A higher shear modulus is desirable for solid-state electrolytes because, as Newman and Monroe estimated, dendritic development can be inhibited at sufficiently high shear moduli. They stated that an electrolyte could prevent dendrites from spreading throughout the solid electrolyte if its shear modulus is more than twice that of lithium metal.^[10,181] It has been discovered that the minimum required shear modulus for dendritic inhibition is around 9 GPa. However, solid polymers possess lower values, making them too soft to prevent dendrite formation. Investigations have shown that lithium dendrite development occurs in these materials.^[182] Sulfides possess minimal mechanical strength. However, with composition and structural optimizations, their shear modulus approaches the threshold value, which should be adequate for limiting dendritic development. Interestingly, compared to other electrolytes, oxides have the highest shear modulus, approximately ten times higher than that of Li metal. Figure 8c illustrates the shear modulus and bulk modulus measurements for different solid-state electrolytes.

The high mechanical strength of oxides may help prevent dendritic development. However, another cause of lithium penetration is inadequate contact between the electrolyte and electrode, often due to fissures across grain boundaries, rather than the mechanical characteristics of oxide electrolytes alone. While the shear modulus is significant, it cannot be the sole factor in determining whether lithium dendrites will develop.^[10,14]

Young's modulus reflects the stiffness of a material, determined by its crystalline structure and chemical bonds.^[183] For instance, sulfides exhibit increased ductility due to reduced bonding energy.^[184] Solid electrolytes typically have a high Young's modulus, making them inherently stiff and brittle. As a result, they are prone to shattering or fracturing under pressure. Additionally, the mechanical characteristics of solid electrolytes can vary significantly depending on the type of solid ceramic used and the material's composition. The Pugh's proportion (B/G) is a method used to assess a material's brittleness.^[185] The Pugh's proportion has a threshold value of 1.74.^[87] Materials with a B/G ratio less than a certain threshold can be classified as brittle. Sulfide solid electrolytes are more ductile than oxides due to their higher B/G ratio. Oxide ceramics, on the other

hand, are brittle and have significant Young's moduli ranging from 100–200 GPa. Specifically, Young's modulus of LLTO, LATP, and LLZO is reported to be approximately 183–200 GPa, 115 GPa, and 140–160 GPa, respectively. Additionally, fracture toughness, denoted by K_C , is another parameter used to assess a material's brittleness, indicating its resistance to the development of fractures. Strong ductile materials possess greater K_C values, and stainless steel exhibits an extremely high K_C value of 70 MPa·(m) $^{1/2}$. Oxide ceramics often have low K_C values of around 1 MPa·(m) $^{1/2}$, further demonstrating that these are very brittle materials.^[10,14]

Crack development and dendritic growth are possible during battery cycling. The ultimate mechanical behavior of SSBs is largely determined by the mechanical characteristics of solid-state electrolytes, which play various roles. A major driving force in the development of SSBs is the suppression of dendritic growth. Ceramic solid-state batteries can address this issue effectively, whereas dendritic growth continues to occur in solid polymer batteries. Despite high shear modulus values in some solid-state batteries, there have been numerous reports of internal short circuits, with evidence suggesting that these issues may be caused by the growth of lithium dendrites within SSEs.^[186] Early research associated grain boundaries in solid-state electrolytes with dendritic development. However, observations of dendritic growth in extremely dense SSEs cast doubt on the role of grain boundaries in dendritic formation. Tasi et al.^[187] verified the significance of surface, dendritic development was thought to be caused by problems with interfacial contact. High local currents caused by inadequate interaction among electrolytes and electrodes ultimately result in dendrite formation. By modifying the interfacial with a gold layer, the durability of the battery may be increased. Further studies by Krauskopf et al. (2019)^[188] showed how the current collector affected the rate of Li dendrite growth. Strong nucleation and heterogeneous lithium deposition can rapidly penetrate Li dendrites and short circuits. Using gold current collectors can slow down dendrite formation by generating a gold-lithium alloy at the junction, thereby improving interfacial contact. These findings highlight the importance of homogeneous lithium plating and close interfacial contact in preventing dendritic penetration. One strategy to prevent lithium dendrite development is to ensure uniform lithium deposition at the interface. Stable mechanical contact is crucial for a mechanically stable solid-state battery. Although achieving components with sufficient mechanical durability and adaptability remains challenging, advanced battery-level concepts are demonstrating practical viability and increasing effectiveness.

5.4. Thermal Sturdiness

One of the main concerns with lithium-ion batteries used in electric vehicles is thermal stability. Compared to liquid electrolytes, solid-state electrolytes have significantly higher breakdown temperatures.^[189] As the temperature rises, various side reactions can lead to the failure or thermal runaway of lithium-ion batteries during operation. Researchers believe that while

SSEs are less prone to volatilization or ignition and typically require high synthetic temperatures, they offer improved thermal stability. SSEs can withstand the high temperatures resulting from internal shorts or other factors, thereby reducing the risk of thermal instability. However, the investigation of the highest temperature limit of thermal sturdiness (T_{ts}) for different types of SSEs is needed today. Generally, T_{ts} symbolize the decomposition temperature. To illustrate the thermal stability of various solid-state electrolytes compared to traditional liquid electrolytes, Figure 8d presents a plot. Among solid-state electrolytes, oxides exhibit the highest thermal stability.^[178] Oxide solid electrolytes are believed to provide the highest thermal stability. According to density functional theory calculations, the degradation temperature of LATP can reach up to 1394 K. Ta-LLZO, on the other hand, exhibits even greater thermal stability, with a degradation temperature of up to 1819 K.^[190] However, Other investigations revealed that LLZO broke down between 1000 and 1250 °C.^[191–193] The system's thermal endurance becomes more complex when solid electrolytes and electrodes are in contact. For example, during heating, oxidation of cathode materials can lead to the degradation of polymer chains. Co-sintering oxide solid electrolytes and electrodes is a common practice to improve interfacial efficiency. However, extreme temperatures can cause decomposition. Therefore, investigating suitable sintering techniques and electrode-electrolyte combinations is crucial for enhancing the thermal stability of oxide interfaces.^[178]

In studies of thermal protection for all-solid-state batteries, it is crucial to consider the thermal safety of the entire battery system, including the materials and interface stability. It has been observed that the breakdown of battery components often leads to overheating. The interaction between the electrolyte and electrode plays a critical role in this process. Internal short circuits within the battery are a primary heat source, generating a substantial amount of heat and causing the internal temperature of a battery pack to rise sharply to 500–600 °C. This places very high demands on the thermal stability of solid-state electrolytes. There are significant variations in the thermal stabilities of solid-state electrolytes. Initial studies focused on the thermal resilience of polymer solid electrolytes, revealing that their ionic conductivity is strongly temperature-dependent, which leads to relatively low decomposition temperatures. In contrast, oxide solid electrolytes, often synthesized at extremely high temperatures, exhibit a high degree of thermal stability.^[178]

6. Interface Engineering

One important factor influencing the adoption of solid-state batteries in real-world industrial applications is the effect of interfaces.^[194] The main obstacle preventing the advancement of oxide SSE-based SSBs is the unfavorable electrode/electrolyte interfaces induced by the stiff oxide solid-state electrolytes.^[75,195,196] Establishing an efficient interface is essential for ensuring optimal electrochemical performance. This section will emphasize the impact of cathode interface design on

electrochemical activity and introduce interface modifications at the anode side.

6.1. At Cathode Side

Interfacial engineering cannot directly influence the ion transport mechanism of a functional cathode. However, it can reduce resistance at the Li^+ /SSE interface.^[21] As previously noted, side reactions between LLZO, water, and carbon dioxide form a Li_2CO_3 layer, which hinders the practical application of LLZO. The production of Li_2CO_3 leads to high interface resistance, which decreases the ionic conductivity of LLZO and reduces the affinity between LLZO and the anode. The Li_2CO_3 layer was observed to be transferred towards an intermediate state known as $\text{Li}_{2.3-x}\text{C}_{0.7+x}\text{B}_{0.3-x}\text{O}_3$ by mixing low melting additive $\text{Li}_{2.3}\text{C}_{0.7}\text{B}_{0.3}\text{O}_3$ (Figure 9a). Increased ionic conductivity in the intermediate state facilitated Li^+ transport at the interface. This additive also has the advantage of a relatively low melting point, making it an excellent adhesive for creating good contact between the cathode and LLZO.^[197] Alexander et al. (2018), employed a successful method to reduce the interface resistance between the NMC cathode and LLZA electrolyte by introducing a Li_2SiO_3 interlayer.^[198] In 2020, Yang et al., applied the Li^+ donating reaction indicating the transformation of the inactive Li_2CO_3 layer to a functional LCO coating layer (Figure 9b).^[199] Considering this, high-efficiency procedures for transforming Li_2CO_3 into a more ionically conductive layer are necessary to improve the functionality of ASSLBs constructed

from garnet-type SSEs. In addition to the Li_2CO_3 conversion process, a low melting point substance can be added to promote Li^+ movement between the solid-state electrolyte and active components by acting as a Li-conducting binder. For instance, Li_3BO_3 has been utilized to enhance the interface between LLCZNO and the LCO cathode.^[200] In a different scenario, the Li_3PO_4 facilitates the continual Li^+ transport routes to the cathode-electrolyte (NMC811-LLZTO) by forming an appropriate Li^+ conductive self-assimilated layer.^[201]

As an alternative, a novel, quick, high-temperature soldering method aided by microwaves was developed to lower interfacial resistance. As shown in Figure 9c, the pure electrode had a porous structure and poor interaction with the cathode materials, leading to high interfacial resistance and unsatisfactory battery performance. However, after only 3 seconds of microwave treatment at 1200 K, all the spaces were filled by molten V_2O_5 , resulting in a dense superstructure with an improved V_2O_5 /garnet interface. When comparing the microwave-treated electrode to the untreated electrode, there was a notable 28.8% decrease in interfacial resistance, falling from $14.4 \text{ k}\Omega/\text{cm}^2$ – $0.5 \text{ k}\Omega/\text{cm}^2$.^[202] Incorporating the positively charged electrode into the solid-state electrolyte as a single unit can reduce the cathode/SSE interface impedance. In sulfide-based solid-state batteries, this is easily accomplished since sulfide SSEs are soft. However, this is challenging in oxide-based SSBs, as oxide SSE ceramics are typically brittle and require higher sintering temperatures. According to Han et al., (2021), the B_2O_3 addition into $\text{Li}_{1.3}\text{Al}_{0.3}\text{Ti}_{1.7}(\text{PO}_4)_3$ electrolyte assists in creating a thin, percolative as well as decreases the

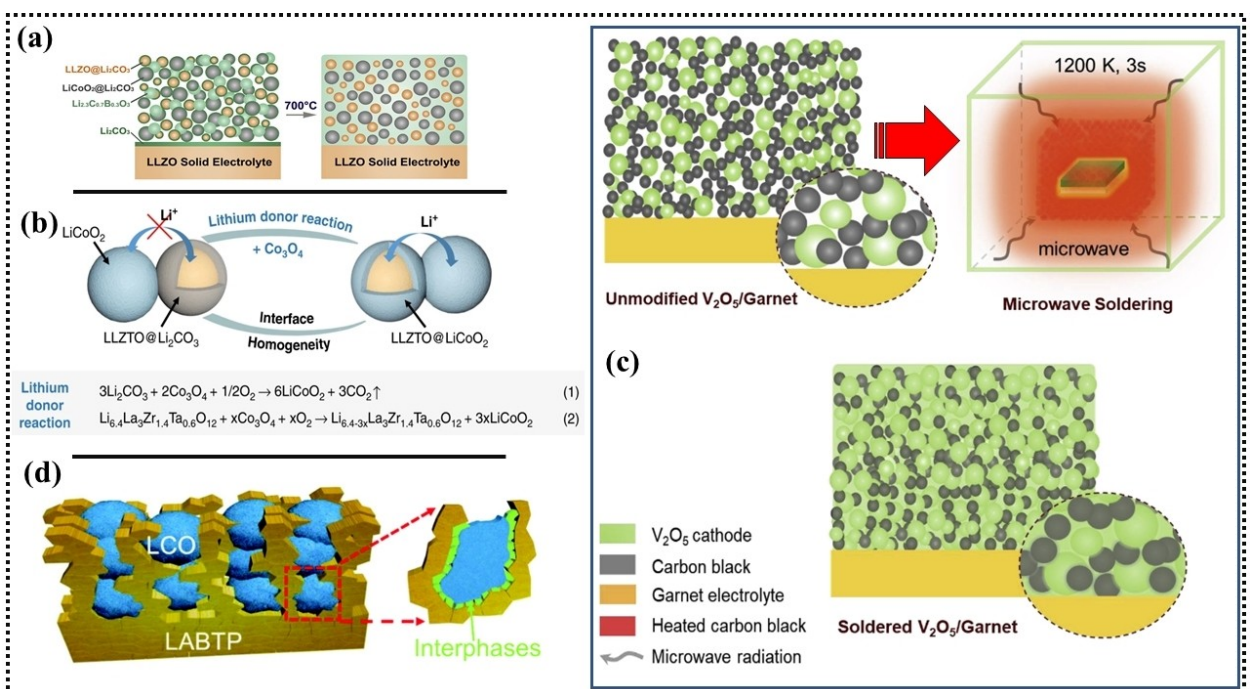


Figure 9. (a) A schematic representation of the interface engineering process to change the Li_2CO_3 to the $\text{Li}_{2.3-x}\text{C}_{0.7+x}\text{B}_{0.3-x}\text{O}_3$ interface. Reprinted with the permission of.^[197] Copyright © 2018, Elsevier. (b) Lithium donor reaction for the transformation of Li_2CO_3 into LCO. Reprinted with the permission of.^[199] Copyright © 2020, Springer Nature. (c) Analysis of untreated and microwave-treated electrode interface and structure. Reprinted with the permission of.^[202] Copyright © 2020, Elsevier. (d) Schematic illustration of interphase formation. Reprinted with the permission of.^[203] Copyright © 2021, The Royal Society of Chemistry.

sintering temperature also develops the hybrid conductive interface between $\text{Li}_{1.3}\text{Al}_{0.3}\text{Ti}_{1.7}(\text{PO}_4)_3$ electrolyte and LiCoO_2 (Figure 9d).^[203] The deployment of oxide solid-state electrolytes for practical applications is hindered by their stiff characteristics, which result in significant interface resistance. Therefore, it is crucial to develop effective methods for creating interfaces with lower interfacial resistance.

Side reactions significantly impact the lifespan and performance of batteries. One of the main problems hindering the development of high-voltage ASSLBs is the side reactions leading to the breakdown of active components and SSEs in solid polymer and sulfide SSE networks, as these materials exhibit low antioxidant capacity.^[204–206] Compared to nitrides and sulfides, Li-containing oxides have stronger antioxidant characteristics. They demonstrate strong stability at voltages greater than 4 V, which makes them promising candidates for functioning as barriers to prevent side reactions. The beneficial effects of Li_xMO_y (where M=Ta, Zr, Si, Nb, etc.) on inhibiting side reactions between solid-state electrolytes and the active ingredients at high voltages have been previously demonstrated. On NMC532, it was discovered that the 10 nm $\text{LiNb}_{0.5}\text{Ta}_{0.5}\text{O}_3$ coating material greatly reduced the side reactions at 4.4 V. It also improved the cyclic stability which supports $\text{LiNb}_{0.5}\text{Ta}_{0.5}\text{O}_3$ role in reducing side reactions. Increasing the electrochemical functionality of ASSLBs requires suitable interface design and carefully chosen coating components. The protective layer must possess strong ionic conductivity and a wide electrochemical stability window to promote Li^+ movement through the interface, inhibit interface reactions, and raise the stable operating voltage.^[207]

6.2. At Anode Side

The anode and the anode/solid-state-electrolyte interface play a crucial role in determining the electrochemical characteristics of ASSLBs. Solid-state electrolytes are often suggested to enable lithium anodes to produce healthier batteries with higher energy densities. However, compared to traditional liquid electrolytes, SSEs can be more prone to lithium dendrite growth, which may lead to rapid short-circuiting of ASSLBs and impede their development.^[208] Inhomogeneous Li^+ transport and uneven charge distribution at the Li/SSE interface are the primary causes of lithium dendrite formation. To mitigate this, creating an effective Li/SSE interface that promotes uniform charge distribution and efficient Li diffusion is crucial. Oxides have recently gained significant attention as a major class of SSEs. Lithium dendrites are less problematic in LATP, LAGP, and LLTO due to potential side reactions between Ti^{4+} or Ge^{4+} and the lithium anode, which can lead to an unreliable Li/SSE interface and excessive potential. However, recent advancements in reducing lithium dendrite development in garnet-type SSEs are noteworthy.

The brittle nature of garnet-type solid-state electrolytes often results in low deformability and a high Young's modulus, leading to inadequate interface contact with the Li anode. Poor surface contact can cause uneven charge distribution, which is

believed to contribute to lithium dendrite formation. To address this issue, researchers have invested significant effort in developing a superior Li/SSE interface to inhibit dendrite formation in garnet-type electrolytes.

As discussed earlier, garnet-type SSEs are known to react with carbon dioxide and water from the environment, resulting in the formation of Li_2CO_3 . When Li_2CO_3 becomes saturated, it transforms the lithiophilic surface into a lithiophobic one, creating a significant gap between the Li anode and the solid-state electrolyte, and leading to high interface resistance.^[164,209,210] There have been reports of many posttreatment techniques to restore the lithiophilic exterior of LLZO and to remove the Li_2CO_3 layer. For example, Li et al., (2018) proposed a simple thermal treatment to remove Li_2CO_3 contamination by treating LLZT using carbon at 700 °C, as shown in Figure 10a. The exterior Li_2CO_3 layer with the H^+ swapped H^+ -LLZT phase in LLZT, prevents Li^+ from migrating through the electrolyte/electrode contact, as a result, the current density is dispersed unevenly, which causes the lithium dendrites to develop quickly. However, The interface resistances of electrolyte, electrolyte/cathode, and electrolyte/Li become extremely tiny in LLZT-C owing to the Li^+ inhibiting layer at the garnet grain's surface being removed. The absence of Li_2CO_3 caused the interface resistance of Li/LLZT-C to decrease from 1210–28 Ω/cm^2 . This was due to a homogeneous charge distribution and excellent interface contact, which allowed for steady Li plating behavior.^[179] Sharafi et al. coupled thermal treatment (500 °C) and wet polishing to produce a Li_2CO_3 -free layer with an extremely low interface resistance ($2 \Omega/\text{cm}^2$) at room temperature.^[164] The incorporation of a stable protective layer is now the accepted method to lower interface impedance and prevent cross-reactions. It is currently shown that Li_3BO_3 is a potentially co-sintering additive that increases the cycle efficiency of SSBs and helps reduce cross-diffusion when heating temperatures as high as 700 °C.^[211] In contrast to garnet-type electrolytes, LAGP/LATP is more susceptible to valence changes with Li^+ metal during electrochemical reactions, highlighting the need for an improved interface protection strategy. As illustrated in Figure 10b, Liu et al. deposited Ge thin film on LAGP, which could simultaneously promote close interaction between Li and LAGP electrolyte and block the inhibition reaction of Ge^{4+} and Li^+ .^[211]

The associated and separated pore structure in the solid electrolyte could be immediately reduced by raising the relative density of the solid electrolyte, which will inhibit the dendritic. One viable strategy to raise relative densities is substituting new synthetic techniques such as hot pressing. In the meantime, adding doping components works well. For instance, LLZO was prepared by hot pressing sintering technique and by solid-state method, the resulting relative densities are 99% and 92.7%, the increased relative density of $\text{Li}_2\text{La}_3\text{Zr}_2\text{O}_{12}$ can effectively prevent lithium dendritic development.^[187] Due to its elevated density, the solid electrolyte possesses fewer linked poles, which effectively inhibits the growth of lithium dendrites. Dense $\text{Li}_2\text{La}_3\text{Zr}_2\text{O}_{12}$ with improved relative density was manufactured using the field-aided sintering process.^[212] It has been demonstrated that using novel sintering methods with dopants

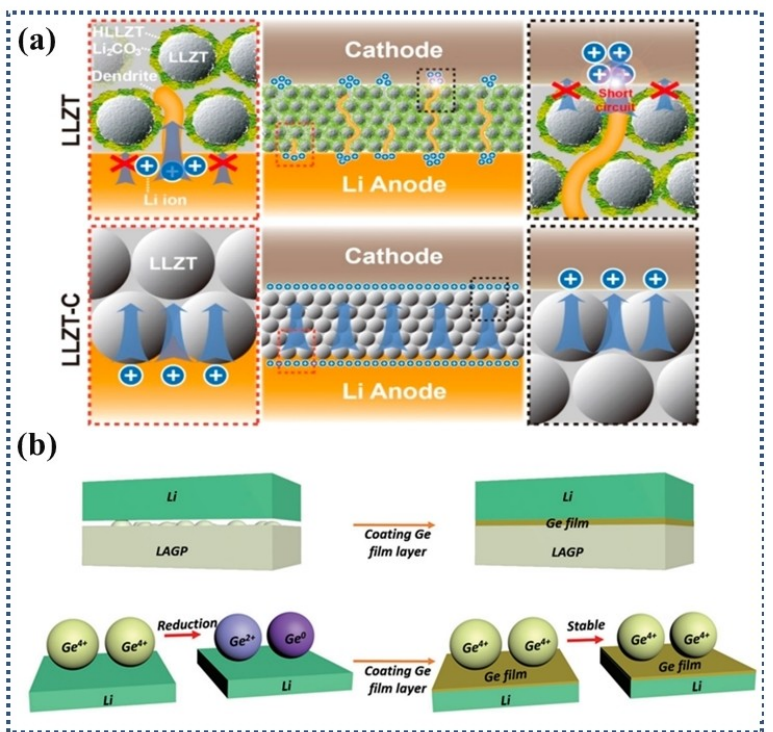


Figure 10. (a) Schematic illustration of garnet LLZT and LLZT–C. Reprinted with the permission of.^[179] Copyright © 2018, American Chemical Society. (b) Schematic representation of the Ge film coating sandwiched between Li and the LAGP. Reprinted with the permission of.^[211] Copyright © 2018 John Wiley and Sons.

to raise the relative density functions well. The lithium dendrites are prevented by the relative density rise, however, there is also a physical contact issue at the interface, which shows high interface impedance. Significant interface impedance occurs when the solid electrolyte and lithium metal contact, mostly due to insufficient contact at the interface. The misaligned lattice of the solid electrolyte, contaminants at the interface, and volumetric variations that the Li metal undergoes during cycling are some of the causes of this resistance. The inadequate wetting characteristics between the solid electrolyte and lithium are triggered by these factors.^[213] The liquid electrolyte may completely wet the electrodes in typical LIBs, ensuring enough contact surface for excellent physical contact. However, in SSBs, the electrolyte and electrodes are solid, they tend to make point-to-point contact with one another. The reaction outcome, Li_2CO_3 , can raise the interface impedance, obstruct the ion transportation channel at the junction, and result in an insulation layer on the contact. Therefore, eliminating surface contaminants can significantly improve physical contact. The following are the remedies for the minimal physical contact and high interface impedance between solid electrolyte and lithium metal: external pressure applying technique, polymer layer-by-layer layout and synthesis, the addition of liquid electrolyte to create smooth contact to address the point-to-point contact, the metallic layer substitution, the inorganic oxide coating method to prevent the gasping effect of lithium metal, and also serves to remove Li_2CO_3 from the LLZO surface to enhance interfacial contact.

The buffer layers introducing method can effectively prevent the formation of lithium dendrites, lessen interface reactions, and increase the wettability of physical contacts.^[214]

7. Conclusions and Perspectives

The development of solid-state lithium-ion batteries has revolutionized the field of energy storage technology and impacted modern society. By replacing traditional liquid electrolytes with solid-state electrolytes, these batteries offer increased energy density and enhanced safety. This review highlights the significant advancements in oxide solid electrolytes for all-solid-state lithium-ion batteries. In summary, the review demonstrates (i) the remarkable progress in developing oxide solid electrolytes and their potential as viable alternatives to traditional liquid electrolytes; (ii) fundamental synthesis methods for solid oxide electrolytes in both bulk and thin-film forms; (iii) a discussion on the key parameters affecting ionic conductivity; (iv) stability challenges in solid-state lithium-ion batteries; and (v) interface issues and their engineering solutions.

Oxide solid electrolytes are categorized into four main types: Garnet, NaSICON, LiSICON, and perovskite materials, each offering unique advantages in terms of stability, safety, and ionic conductivity. Despite significant advancements, several challenges remain, including manufacturing scalability for large-scale industrial applications, moisture stability, and improvements in electrochemical performance. Considering these issues

and challenges, potential pathways and opportunities for high-energy-density solid-state lithium batteries can be summarized as follows:

- i) Ongoing efforts to explore and manufacture novel materials are crucial for identifying oxide solid-state electrolytes with enhanced electrochemical properties. As SSBs with high energy density, robust thermal stability, and safe operational characteristics move closer to commercialization, ionic conductivity remains a key factor in determining the suitability of a material as a solid electrolyte. Although ionic conductivity is no longer the primary bottleneck for certain solid-state lithium-ion batteries, enhancing Li^+ ion conductivity and reducing electronic conductivity are still essential for achieving rapid charging across all temperatures. A comprehensive investigation into crystalline structures, migration pathways, and lithium-ion transport processes is necessary to improve ionic conductivity. Considerable attention should be given to designing fast diffusion paths and optimizing the surrounding contacts for Li ions. Developing superionic conductive structural frameworks could advance the field of SSEs. Additionally, employing high-entropy mechanisms to boost ionic conductivity and increasing Li^+ concentration may lead to more favorable Li^+ arrangements and easier ion movement in high-energy sites.
 - ii) To fully realize the benefits of oxide solid-state electrolytes, it is essential to optimize manufacturing procedures and scale up production methods. Despite the challenges associated with sintering electrolytes, efficient and cost-effective solution-based approaches have been explored for synthesizing ceramic SSEs, though their adoption has been limited. For optimal ionic conductivity, SSEs must be sintered for several hours at temperatures ranging from 600 °C–1100 °C. However, prolonged sintering often leads to significant loss of Li and Na. Traditional ceramic synthesis methods commonly address this by either lowering the temperature to minimize Li loss or by adding extra Li to compensate, which can sometimes result in poor compositional control and a porous structure. There remains a need for scalable processes that achieve precise compositional accuracy and high crystallinity to attain the desired ionic conductivities. Developing unconventional heat treatments, such as rapid sintering, could be a promising approach. This technique allows for the formation of a dense, polycrystalline framework with minimal loss of volatile elements. Collaboration between academic institutions, industry, and government organizations is crucial to expedite the transition from lab-scale prototypes to practical all-solid-state lithium-ion batteries.
 - iii) Designing effective solid electrolyte/electrode interfaces and incorporating artificial protective layers are common techniques to enhance the electrochemical efficiency and interfacial strength of all-solid-state lithium-ion batteries. Inadequate electrode-electrolyte contact exacerbates interface issues. Improving the interface compatibility between oxide SEs and electrodes, especially with lithium metal anodes, is crucial and requires further investigation. Techniques such as adding interface protective layers, employing multipurpose ion doping, and creating hybrid structures are effective strategies to prevent SE deterioration. The solid-state battery sector should focus on characterizing and developing passivation interphases between solid electrolytes and electrodes. Typically, oxide electrolytes are examined in their flat, planar form, where the electrolyte powder is sintered into uniformly high-density pellets with good conductivity and durability. However, the planar shape restricts electrode interaction to the geometrical contact region, contributing to high interface impedance. To address this, researchers might explore interface physical structure designs, such as interdigititation structures or multi-layer electrolyte configurations, to create anchoring effects and enhance compatibility. Additionally, improving interface stability through welding technologies, such as ultrasonic welding, could be beneficial.
 - iv) The mechanical properties of solid-state lithium-ion batteries significantly impact their extended cyclability. While chemical and electrochemical stability are crucial, mechanical stability is equally important for ensuring long-term performance. However, systematic research on the mechanical effects and their relationship to the electromechanical functioning of SSLBs is limited. This area requires further investigation to understand how mechanical factors influence the overall performance and durability of SSLBs.
 - v) The thickness of the solid electrolyte is closely linked to the energy density of the battery. Therefore, developing advanced thin film preparation technologies is essential to achieve thinner electrolyte layers, which can enhance the overall energy density of solid-state lithium-ion batteries.
 - vi) Manufactured solid electrolytes should be economically viable, cost-effective, environmentally friendly, and energy-efficient, while also maintaining high quality.
- Overall, while oxide solid electrolytes demonstrate significant advantages, practical application in all-solid-state battery systems remains challenging. Future efforts should focus on comprehensive studies that integrate advanced technical methods and characterization strategies. The goal is to enable the large-scale commercial deployment of ASSBs based on oxide solid electrolytes, achieving broad operating temperature ranges, high energy densities, and long-term stability.

Acknowledgements

This work was financially supported by Shenzhen Science and Technology Program (Grant No. KQTD20200820113045083, ZDSYS20190902093220279, JCYJ20220818102403007), Shenzhen Research Fund for Returned Scholars (DD11409017).

Conflict of Interests

The authors declare no conflict of interest.

Keywords: Oxide solid electrolytes • Solid-state batteries • Ionic conductivity • Stability issues

- [1] N. Boaretto, I. Garbayo, S. Valiyaveettil-SobhanRaj, A. Quintela, C. Li, M. Casas-Cabanás, F. Aguesse, *J. Power Sources* **2021**, *502*, 229919.
- [2] J. Janek, W. G. Zeier, *Nat. Energy* **2023**, *8*, 230–240.
- [3] W. Zhao, J. Yi, P. He, H. Zhou, *Electrochem. Energy Rev.* **2019**, *2*, 574–605.
- [4] T. Famprikis, P. Canepa, J. A. Dawson, M. S. Islam, C. Masquelier, *Nat. Mater.* **2019**, *18*, 1278–1291.
- [5] A. J. Niri, G. A. Poelzer, S. E. Zhang, J. Rosenkranz, M. Pettersson, Y. Ghorbani, *Renewable Sustainable Energy Rev.* **2024**, *191*, 114176.
- [6] T. Kim, W. Song, D.-Y. Son, L. K. Ono, Y. Qi, *J. Mater. Chem. A* **2019**, *7*, 2942–2964.
- [7] S. Zhou, M. Li, P. Wang, L. Cheng, L. Chen, Y. Huang, S. Yu, F. Mo, J. Wei, *Electrochem. Energy Rev.* **2023**, *6*, 34.
- [8] B. He, F. Zhang, Y. Xin, C. Xu, X. Hu, X. Wu, Y. Yang, H. Tian, *Nat. Chem. Rev.* **2023**, *7*, 826–842.
- [9] R. Wei, S. Chen, T. Gao, W. Liu, *Nano Select* **2021**, *2*, 2256–2274.
- [10] R. Chen, Q. Li, X. Yu, L. Chen, H. Li, *Chem. Rev.* **2019**, *120*, 6820–6877.
- [11] Q. Wang, P. Ping, X. Zhao, G. Chu, J. Sun, C. Chen, *J. Power Sources* **2012**, *208*, 210–224.
- [12] J. Chen, J. Wu, X. Wang, Z. Yang, *Energy Storage Mater.* **2021**, *35*, 70–87.
- [13] Z. Zhang, X. Wang, X. Li, J. Zhao, G. Liu, W. Yu, X. Dong, J. Wang, *Mater. Today Sustain.* **2023**, *21*, 100316.
- [14] K. J. Kim, M. Balaish, M. Wadaguchi, L. Kong, J. L. Rupp, *Adv. Energy Mater.* **2021**, *11*, 2002689.
- [15] J. Liu, Z. Bao, Y. Cui, E. J. Dufek, J. B. Goodenough, P. Khalifah, Q. Li, B. Y. Liaw, P. Liu, A. Manthiram, *Nat. Energy* **2019**, *4*, 180–186.
- [16] F. Liang, Y. Sun, Y. Yuan, J. Huang, M. Hou, J. Lu, *Mater. Today* **2021**, *50*, 418–441.
- [17] J. W. Choi, D. Aurbach, *Nat. Rev. Mater.* **2016**, *1*, 1–16.
- [18] Z. Ma, J. Chen, J. Vatamanu, O. Borodin, D. Bedrov, X. Zhou, W. Zhang, W. Li, K. Xu, L. Xing, *Energy Storage Mater.* **2022**, *45*, 903–910.
- [19] J. Schnell, T. Günther, T. Knoche, C. Vieider, L. Köhler, A. Just, M. Keller, S. Passerini, G. Reinhart, *J. Power Sources* **2018**, *382*, 160–175.
- [20] A. Manthiram, X. Yu, S. Wang, *Nat. Rev. Mater.* **2017**, *2*, 1–16.
- [21] P. Jiang, G. Du, J. Cao, X. Zhang, C. Zou, Y. Liu, X. Lu, *Energy Technol.* **2023**, *11*, 2201288.
- [22] D. Wu, L. Chen, H. Li, F. Wu, *Prog. Mater. Sci.* **2023**, *139*, 101182.
- [23] J. Yan, D. Zhu, H. Ye, H. Sun, X. Zhang, J. Yao, J. Chen, L. Geng, Y. Su, P. Zhang, *ACS Energy Lett.* **2022**, *7*, 3855–3863.
- [24] Z. Gao, H. Sun, L. Fu, F. Ye, Y. Zhang, W. Luo, Y. Huang, *Adv. Mater.* **2018**, *30*, 1705702.
- [25] T. Ye, L. Li, Y. Zhang, *Adv. Funct. Mater.* **2020**, *30*, 2000077.
- [26] M. V. Reddy, C. M. Julien, A. Mauger, K. Zaghib, *Nanomaterials* **2020**, *10*, 1606.
- [27] J. Kriegler, M. Finsterbusch, Y. Liang, E. Jaimez-Farnham, M. F. Zaeh, *J. Power Sources* **2024**, *596*, 234091.
- [28] A. M. Ralls, K. Leong, J. Clayton, P. Fuelling, C. Mercer, V. Navarro, P. L. Menezes, *Materials (Basel)* **2023**, *16*, 6063.
- [29] X. Yang, K. R. Adair, X. Gao, X. Sun, *Energy Environ. Sci.* **2021**, *14*, 643–671.
- [30] P. Mandade, M. Weil, M. Baumann, Z. Wei, *Chem. Eng. J. Adv.* **2023**, *13*, 100439.
- [31] X. Gao, M. Zheng, X. Yang, R. Sun, J. Zhang, X. Sun, *Mater. Today* **2022**, *59*, 161–181.
- [32] H. Yang, M. Jing, L. Wang, H. Xu, X. Yan, X. He, *Nano-Micro Lett.* **2024**, *16*, 1–33.
- [33] A. Machín, C. Morant, F. Márquez, *Batteries* **2024**, *10*, 29.
- [34] S. Huang, P. Cao, in *Advanced Ceramics for Energy Storage, Thermoelectrics and Photonics*, Elsevier, Amsterdam, **2023**, pp. 77–117.
- [35] H. Yang, N. Wu, *Energy Sci. Eng.* **2022**, *10*, 1643–1671.
- [36] S. Chai, Q. He, J. Zhou, Z. Chang, A. Pan, H. Zhou, *ChemSusChem* **2024**, *17*, e202301268.
- [37] Y. Xiao, Y. Wang, S.-H. Bo, J. C. Kim, L. J. Miara, G. Ceder, *Nat. Rev. Mater.* **2020**, *5*, 105–126.
- [38] L. Devaraj, S. V. Thummalapalli, N. Fonseca, H. Nazir, K. Song, A. M. Kannan, *Mater. Today Sustain.* **2023**, *25*, 100614.
- [39] Y. Gao, X. Wang, W. Wang, Q. Fang, *Solid State Ionics* **2010**, *181*, 33–36.
- [40] C. Shao, H. Liu, Z. Yu, Z. Zheng, N. Sun, C. Diao, *Solid State Ionics* **2016**, *287*, 13–16.
- [41] R. Murugan, V. Thangadurai, W. Weppner, *Angew. Chem. Int. Ed. Engl.* **2007**, *46*, 7778.
- [42] Y. Li, J.-T. Han, C.-A. Wang, H. Xie, J. B. Goodenough, *J. Mater. Chem.* **2012**, *22*, 15357–15361.
- [43] C. Deviannapoorani, L. Dhivya, S. Ramakumar, R. Murugan, *J. Power Sources* **2013**, *240*, 18–25.
- [44] L. Buannic, B. Orayech, J.-M. Lopez Del Amo, J. Carrasco, N. A. Katcho, F. D. R. Aguesse, W. Manalastas, W. Zhang, J. Kilner, A. Llóredés, *Chem. Mater.* **2017**, *29*, 1769–1778.
- [45] S. Qin, X. Zhu, Y. Jiang, M. E. Ling, Z. Hu, J. Zhu, *Appl. Phys. Lett.* **2018**, *112*, 113901.
- [46] L. H. Abrha, T. T. Hagos, Y. Nikodimos, H. K. Bezabih, G. B. Berhe, T. M. Hagos, C.-J. Huang, W. A. Tegenge, S.-K. Jiang, H. H. Weldeyohannes, *ACS Appl. Mater. Interfaces* **2020**, *12*, 25709–25717.
- [47] Y. Chen, T. Wang, H. Chen, W. H. Kan, W. Yin, Z. Song, C. Wang, J. Ma, W. Luo, Y. Huang, *Matter* **2023**, *6*, 1530–1541.
- [48] Z. Fu, J. Ferguson, *J. Am. Ceram. Soc.* **2022**, *105*, 6175–6183.
- [49] S. Narayanan, S. Reid, S. Butler, V. Thangadurai, *Solid State Ionics* **2019**, *331*, 22–29.
- [50] S. Song, H. M. Duong, A. M. Korsunsky, N. Hu, L. Lu, *Sci. Rep.* **2016**, *6*, 32330.
- [51] Y. Lu, J. A. Alonso, Q. Yi, L. Lu, Z. L. Wang, C. Sun, *Adv. Energy Mater.* **2019**, *9*, 1901205.
- [52] Q. Zhang, F. Liang, T. Qu, Y. Yao, W. Ma, B. Yang, Y. Dai, in *IOP Conference Series: Materials Science and Engineering*, Vol. 423, IOP Publishing **2018**, p. 012122.
- [53] Z. Zhang, Z. Zou, K. Kaup, R. Xiao, S. Shi, M. Avdeev, Y. S. Hu, D. Wang, B. He, H. Li, *Adv. Energy Mater.* **2019**, *9*, 1902373.
- [54] S. K. Pal, R. Saha, G. V. Kumar, S. Omar, *J. Phys. Chem. C* **2020**, *124*, 9161–9169.
- [55] A. Martinez-Juarez, C. Pecharromán, J. E. Iglesias, J. M. Rojo, *J. Phys. Chem. B* **1998**, *102*, 372–375.
- [56] H. Aono, E. Sugimoto, Y. Sadaoka, N. Imanaka, G. Y. Adachi, *J. Electrochem. Soc.* **1990**, *137*, 1023.
- [57] P. Bharathi, S.-F. Wang, *ACS Appl. Nano Mater.* **2024**, *7*, 1615–1624.
- [58] J. Feng, L. Lu, M. Lai, *J. Alloys Compd.* **2010**, *501*, 255–258.
- [59] M. Illbeigi, A. Fazlali, M. Kazazi, A. H. Mohammadi, *Solid State Ionics* **2016**, *289*, 180–187.
- [60] J. Kuwano, A. West, *Mater. Res. Bull.* **1980**, *15*, 1661–1667.
- [61] J. C. Bachman, S. Muy, A. Grimaud, H.-H. Chang, N. Pour, S. F. Lux, O. Paschos, F. Maglia, S. Lupart, P. Lamp, *Chem. Rev.* **2016**, *116*, 140–162.
- [62] P. G. Bruce, A. West, *J. Electrochem. Soc.* **1983**, *130*, 662.
- [63] M. Dissanayake, R. Gunawardane, H. Sumathipala, A. West, *Solid State Ionics* **1995**, *76*, 215–220.
- [64] S. Song, J. Lu, F. Zheng, H. M. Duong, L. Lu, *RSC Adv.* **2015**, *5*, 6588–6594.
- [65] E. Gilardi, G. Materzanini, L. Kahle, M. Dobeli, S. Lacey, X. Cheng, N. Marzari, D. Pergolesi, A. Hintennach, T. Lippert, *ACS Appl. Energ. Mater.* **2020**, *3*, 9910–9917.
- [66] Y. Deng, C. Eames, B. Fleutot, R. David, J.-N. Chotard, E. Suard, C. Masquelier, M. S. Islam, *ACS Appl. Mater. Interfaces* **2017**, *9*, 7050–7058.
- [67] Y. Inaguma, C. Liqian, M. Itoh, T. Nakamura, T. Uchida, H. Ikuta, M. Wakihara, *Solid State Commun.* **1993**, *86*, 689–693.
- [68] V. Thangadurai, A. Shukla, J. Gopalakrishnan, *Chem. Mater.* **1999**, *11*, 835–839.
- [69] R. Inada, K. Kimura, K. Kusakabe, T. Tojo, Y. Sakurai, *Solid State Ionics* **2014**, *261*, 95–99.
- [70] B. Huang, B. Xu, Y. Li, W. Zhou, Y. You, S. Zhong, C.-A. Wang, J. B. Goodenough, *ACS Appl. Mater. Interfaces* **2016**, *8*, 14552–14557.
- [71] H. T. Le, R. S. Kalubarme, D. T. Ngo, S.-Y. Jang, K.-N. Jung, K.-H. Shin, C.-J. Park, *J. Power Sources* **2015**, *274*, 1188–1199.
- [72] S.-J. Lee, J.-J. Bae, J.-T. Son, *J. Korean Phys. Soc.* **2019**, *74*, 73–77.
- [73] A. Morata-Orrantia, S. García-Martín, E. Morán, M. Á. Alario-Franco, *Chem. Mater.* **2002**, *14*, 2871–2875.
- [74] V. Thangadurai, S. Narayanan, D. Pinzaru, *Chem. Soc. Rev.* **2014**, *43*, 4714–4727.
- [75] C. Wang, K. Fu, S. P. Kammampata, D. W. McOwen, A. J. Samson, L. Zhang, G. T. Hitz, A. M. Nolan, E. D. Wachsman, Y. Mo, *Chem. Rev.* **2020**, *120*, 4257–4300.
- [76] M. P. O'Callaghan, A. S. Powell, J. J. Titman, G. Z. Chen, E. J. Cussen, *Chem. Mater.* **2008**, *20*, 2360–2369.
- [77] M. P. O'Callaghan, D. R. Lynham, E. J. Cussen, G. Z. Chen, *Chem. Mater.* **2006**, *18*, 4681–4689.
- [78] V. Thangadurai, W. Weppner, *Adv. Funct. Mater.* **2005**, *15*, 107–112.

- [79] R. Murugan, V. Thangadurai, W. Weppner, *Angew. Chem. Int. Ed.* **2007**, *46*, 7778–7781.
- [80] E. J. Cussen, *J. Mater. Chem.* **2010**, *20*, 5167–5173.
- [81] K. Kataoka, H. Nagata, J. Akimoto, *Sci. Rep.* **2018**, *8*, 9965.
- [82] V. Thangadurai, H. Kaack, W. J. Weppner, *J. Am. Ceram. Soc.* **2003**, *86*, 437–440.
- [83] Y. Ren, T. Danner, A. Moy, M. Finsterbusch, T. Hamann, J. Dippell, T. Fuchs, M. Müller, R. Hoft, A. Weber, *Adv. Energy Mater.* **2023**, *13*, 2201939.
- [84] Q. Liu, Z. Geng, C. Han, Y. Fu, S. Li, Y.-B. He, F. Kang, B. Li, *J. Power Sources* **2018**, *389*, 120–134.
- [85] N. Zhao, W. Khokhar, Z. Bi, C. Shi, X. Guo, L.-Z. Fan, C.-W. Nan, *Joule* **2019**, *3*, 1190–1199.
- [86] J. E. Ni, E. D. Case, J. S. Sakamoto, E. Rangasamy, J. B. Wolfenstine, *J. Mater. Sci.* **2012**, *47*, 7978–7985.
- [87] S. Yu, R. D. Schmidt, R. Garcia-Mendez, E. Herbert, N. J. Dudney, J. B. Wolfenstine, J. Sakamoto, D. J. Siegel, *Chem. Mater.* **2016**, *28*, 197–206.
- [88] A. Kim, S. Woo, M. Kang, H. Park, B. Kang, *Front. Chem.* **2020**, *8*, 468.
- [89] W. D. Richards, L. J. Miara, Y. Wang, J. C. Kim, G. Ceder, *Chem. Mater.* **2016**, *28*, 266–273.
- [90] J. B. Goodenough, H.-P. Hong, J. Kafalas, *Mater. Res. Bull.* **1976**, *11*, 203–220.
- [91] H.-P. Hong, *Mater. Res. Bull.* **1976**, *11*, 173–182.
- [92] V. Thangadurai, W. Weppner, *Ionics* **2006**, *12*, 81–92.
- [93] L. Shen, J. Yang, G. Liu, M. Avdeev, X. Yao, *Mater. Today Energy* **2021**, *20*, 100691.
- [94] J. Boilot, J. Salanie, G. Desplanches, D. Le Potier, *Mater. Res. Bull.* **1979**, *14*, 1469–1477.
- [95] U. Von Alpen, M. Bell, W. Wichelhaus, *Mater. Res. Bull.* **1979**, *14*, 1317–1322.
- [96] A. G. Jolley, D. D. Taylor, N. J. Schreiber, E. D. Wachsman, *J. Am. Ceram. Soc.* **2015**, *98*, 2902–2907.
- [97] C. Li, R. Li, K. Liu, R. Si, Z. Zhang, Y. S. Hu, *Interd. Mater.* **2022**, *1*, 396–416.
- [98] Y. Wang, S. Song, C. Xu, N. Hu, J. Molenda, L. Lu, *Nano Mater. Sci.* **2019**, *1*, 91–100.
- [99] M. Hou, F. Liang, K. Chen, Y. Dai, D. Xue, *Nanotechnology* **2020**, *31*, 132003.
- [100] R. DeWees, H. Wang, *ChemSusChem* **2019**, *12*, 3713–3725.
- [101] J. Fu, *Solid State Ionics* **1997**, *96*, 195–200.
- [102] J. Fu, *Solid State Ionics* **1997**, *104*, 191–194.
- [103] H.-P. Hong, *Mater. Res. Bull.* **1978**, *13*, 117–124.
- [104] Z. Zulfiqar, S. Zulfiqar, Q. Abbas, M. Mirzaeian, R. Raza, *Energy Storage* **2023**, *6*(1), e506.
- [105] B. Tao, C. Ren, H. Li, B. Liu, X. Jia, X. Dong, S. Zhang, H. Chang, *Adv. Funct. Mater.* **2022**, *32*, 2203551.
- [106] P. Bruce, A. West, *J. Solid State Chem.* **1982**, *44*, 354–365.
- [107] T. Takahashi, H. Iwahara, *Energy Convers.* **1971**, *11*, 105–111.
- [108] J. Lu, Y. Li, *J. Mater. Sci. Mater. Electron.* **2021**, *32*, 9736–9754.
- [109] J. Lu, Y. Li, Y. Ding, *JOM* **2020**, *72*, 3256–3261.
- [110] K. Mitsuishi, T. Ohnishi, Y. Tanaka, K. Watanabe, I. Sakaguchi, N. Ishida, M. Takeguchi, T. Ohno, D. Fujita, K. Takada, *Appl. Phys. Lett.* **2012**, *101*, 073903.
- [111] S. Stramare, V. Thangadurai, W. Weppner, *Chem. Mater.* **2003**, *15*, 3974–3990.
- [112] S. Yan, C.-H. Yim, V. Pankov, M. Bauer, E. Baranova, A. Weck, A. Merati, Y. Abu-Lebdeh, *Batteries* **2021**, *7*, 75.
- [113] Y. Harada, T. Ishigaki, H. Kawai, J. Kuwano, *Solid State Ionics* **1998**, *108*, 407–413.
- [114] C. Chen, S. Xie, E. Sperling, A. Yang, G. Henriksen, K. Amine, *Solid State Ionics* **2004**, *167*, 263–272.
- [115] W. J. Kwon, H. Kim, K.-N. Jung, W. Cho, S. H. Kim, J.-W. Lee, M.-S. Park, *J. Mater. Chem. A* **2017**, *5*, 6257–6262.
- [116] L. Cheng, W. Chen, M. Kunz, K. Persson, N. Tamura, G. Chen, M. Doeff, *ACS Appl. Mater. Interfaces* **2015**, *7*, 2073–2081.
- [117] M. Wood, X. Gao, R. Shi, T. W. Heo, J. A. Espitia, E. B. Duoss, B. C. Wood, J. Ye, *J. Power Sources* **2021**, *484*, 229252.
- [118] S. Ramakumar, C. Deviannapoorani, L. Dhivya, L. S. Shankar, R. Murugan, *Prog. Mater. Sci.* **2017**, *88*, 325–411.
- [119] L. L. Hench, J. K. West, *Chem. Rev.* **1990**, *90*, 33–72.
- [120] A. E. Danks, S. R. Hall, Z. Schnepf, *Mater. Horiz.* **2016**, *3*, 91–112.
- [121] R. R. Tummala, *J. Am. Ceram. Soc.* **1991**, *74*, 895–908.
- [122] A. Hayashi, K. Minami, F. Mizuno, M. Tatsumisago, *J. Mater. Sci.* **2008**, *43*, 1885–1889.
- [123] S. Gółowniak, B. Szczęśniak, J. Choma, M. Jaroniec, *Adv. Mater.* **2021**, *33*, 2103477.
- [124] A. Zaker, Z. Chen, X. Wang, Q. Zhang, *Fuel Process. Technol.* **2019**, *187*, 84–104.
- [125] M. Amores, T. E. Ashton, P. J. Baker, E. J. Cussen, S. A. Corr, *J. Mater. Chem. A* **2016**, *4*, 1729–1736.
- [126] D. Zuo, L. Yang, Z. Zou, S. Li, Y. Feng, S. J. Harris, S. Shi, J. Wan, *Adv. Energy Mater.* **2023**, *13*, 2301540.
- [127] C. Wang, W. Ping, Q. Bai, H. Cui, R. Hensleigh, R. Wang, A. H. Brozena, Z. Xu, J. Dai, Y. Pei, *Science* **2020**, *368*, 521–526.
- [128] S. Chen, L. Nie, X. Hu, Y. Zhang, Y. Zhang, Y. Yu, W. Liu, *Adv. Mater.* **2022**, *34*, 2200430.
- [129] Y. Feng, L. Yang, Z. Yan, D. Zuo, Z. Zhu, L. Zeng, Y. Zhu, J. Wan, *Energy Storage Mater.* **2023**, *63*, 103053.
- [130] X. Hu, D. Zuo, S. Cheng, S. Chen, Y. Liu, W. Bao, S. Deng, S. J. Harris, J. Wan, *Chem. Soc. Rev.* **2023**, *52*, 1103–1128.
- [131] M. Zhang, Z. Huang, J. Cheng, O. Yamamoto, N. Imanishi, B. Chi, J. Pu, J. Li, *J. Alloys Compd.* **2014**, *590*, 147–152.
- [132] S. Lobe, C. Dellen, M. Finsterbusch, H.-G. Gehrke, D. Sebold, C.-L. Tsai, S. Uhlenbrück, O. Guillou, *J. Power Sources* **2016**, *307*, 684–689.
- [133] K. Xu, *Chem. Rev.* **2004**, *104*, 4303–4418.
- [134] J. B. Goodenough, *Annu. Rev. Mater. Res.* **2003**, *33*, 91–128.
- [135] R. P. Buck, *Sensor. Actuat.* **1981**, *1*, 137–196.
- [136] X. He, Y. Zhu, Y. Mo, *Nat. Commun.* **2017**, *8*, 15893.
- [137] Y. Wang, W. D. Richards, S. P. Ong, L. J. Miara, J. C. Kim, Y. Mo, G. Ceder, *Nat. Mater.* **2015**, *14*, 1026–1031.
- [138] B. Zhang, R. Tan, L. Yang, J. Zheng, K. Zhang, S. Mo, Z. Lin, F. Pan, *Energy Storage Mater.* **2018**, *10*, 139–159.
- [139] A. Van der Ven, J. Bhattacharya, A. A. Belak, *Acc. Chem. Res.* **2013**, *46*, 1216–1225.
- [140] J. Souquet, *Annu. Rev. Mater. Sci.* **1981**, *11*, 211–231.
- [141] J. Gao, Y.-S. Zhao, S.-Q. Shi, H. Li, *Chin. Phys. B* **2015**, *25*, 018211.
- [142] M. Wagemaker, G. J. Kearley, A. A. Van Well, H. Mutka, F. M. Mulder, *J. Am. Chem. Soc.* **2003**, *125*, 840–848.
- [143] S. Lee, D. Lee, A. Manthiram, *J. Mater. Chem. A* **2024**, *12*, 26244–26252.
- [144] L. Zhao, Q. Dong, R. Yi, H. Shao, Y. Shen, L. Chen, *CCS Chem.* **2024**, *6*, 1–57.
- [145] J. Yan, J. Yu, B. Ding, *Adv. Mater.* **2018**, *30*, 1705105.
- [146] S. Mukhopadhyay, T. Thompson, J. Sakamoto, A. Huq, J. Wolfenstine, J. L. Allen, N. Bernstein, D. A. Stewart, M. Johannes, *Chem. Mater.* **2015**, *27*, 3658–3665.
- [147] S. Xia, X. Wu, Z. Zhang, Y. Cui, W. Liu, *Chem* **2019**, *5*, 753–785.
- [148] L. J. Miara, W. D. Richards, Y. E. Wang, G. Ceder, *Chem. Mater.* **2015**, *27*, 4040–4047.
- [149] Y. Jin, P. J. McGinn, *J. Power Sources* **2011**, *196*, 8683–8687.
- [150] S. Ohta, T. Kobayashi, T. Asaoka, *J. Power Sources* **2011**, *196*, 3342–3345.
- [151] K. Hayamizu, Y. Matsuda, M. Matsui, N. Imanishi, *Solid State Nucl. Magn. Reson.* **2015**, *70*, 21–27.
- [152] R.-H. Shin, S.-I. Son, S.-M. Lee, Y. S. Han, Y. D. Kim, S.-S. Ryu, *J. Korean Ceram. Soc.* **2016**, *53*(6), 712–718.
- [153] Y. Inaguma, L. Chen, M. Itoh, T. Nakamura, *Solid State Ionics* **1994**, *70*, 196–202.
- [154] F. Zheng, M. Kotobuki, S. Song, M. O. Lai, L. Lu, *J. Power Sources* **2018**, *389*, 198–213.
- [155] Y. Li, M. Li, Z. Sun, Q. Ni, H. Jin, Y. Zhao, *Energy Storage Mater.* **2023**, *56*, 582–599.
- [156] C. Liang, *J. Electrochem. Soc.* **1973**, *120*, 1289.
- [157] S. C. Singhal, K. Kendall, *High-Temperature Solid Oxide Fuel Cells: Fundamentals, Design and Applications*, Elsevier, Amsterdam, 2003.
- [158] S. R. Hui, J. Roller, S. Yick, X. Zhang, C. Decès-Petit, Y. Xie, R. Maric, D. Ghosh, *J. Power Sources* **2007**, *172*, 493–502.
- [159] H. Maekawa, R. Tanaka, T. Sato, Y. Fujimaki, T. Yamamura, *Solid State Ionics* **2004**, *175*, 281–285.
- [160] H. Maekawa, T. Iwatanai, H. Shen, T. Yamamura, J. Kawamura, *Solid State Ionics* **2008**, *178*, 1637–1641.
- [161] D. Simon, E. Kelder, M. Wagemaker, F. Mulder, J. Schoonman, *Solid State Ionics* **2006**, *177*, 2759–2768.
- [162] L. Cheng, E. J. Crumlin, W. Chen, R. Qiao, H. Hou, S. F. Lux, V. Zorba, R. Russo, R. Kostecki, Z. Liu, *Phys. Chem. Chem. Phys.* **2014**, *16*, 18294–18300.
- [163] W. Xia, B. Xu, H. Duan, X. Tang, Y. Guo, H. Kang, H. Li, H. Liu, *J. Am. Ceram. Soc.* **2017**, *100*, 2832–2839.
- [164] A. Sharafi, E. Kazyak, A. L. Davis, S. Yu, T. Thompson, D. J. Siegel, N. P. Dasgupta, J. Sakamoto, *Chem. Mater.* **2017**, *29*, 7961–7968.

- [165] Y. Jin, P. J. McGinn, *J. Power Sources* **2013**, *239*, 326–331.
- [166] T. Durán, E. Climent-Pascual, M. T. Pérez-Prior, B. Levenfeld, A. Varez, I. Sobrados, J. Sanz, *Adv. Powder Technol.* **2017**, *28*, 514–520.
- [167] Y. Li, B. Xu, H. Xu, H. Duan, X. Lü, S. Xin, W. Zhou, L. Xue, G. Fu, A. Manthiram, *Angew. Chem. Int. Ed.* **2017**, *56*, 753–756.
- [168] C. Galven, J. Dittmer, E. Suard, F. Le Berre, M.-P. Crosnier-Lopez, *Chem. Mater.* **2012**, *24*, 3335–3345.
- [169] J.-F. Wu, B.-W. Pu, D. Wang, S.-Q. Shi, N. Zhao, X. Guo, X. Guo, *ACS Appl. Mater. Interfaces* **2018**, *11*, 898–905.
- [170] Y. Zhu, X. He, Y. Mo, *J. Mater. Chem. A* **2016**, *4*, 3253–3266.
- [171] M. Nakayama, M. Kotobuki, H. Munakata, M. Nogami, K. Kanamura, *Phys. Chem. Chem. Phys.* **2012**, *14*, 10008–10014.
- [172] F. Han, Y. Zhu, X. He, Y. Mo, C. Wang, *Adv. Energy Mater.* **2016**, *6*, 1501590.
- [173] R. Xu, Z. Wu, S. Zhang, X. Wang, Y. Xia, X. Xia, X. Huang, J. Tu, *Chem. A Eur. J.* **2017**, *23*, 13950–13956.
- [174] S. G. Kang, D. S. Sholl, *J. Phys. Chem. C* **2014**, *118*, 17402–17406.
- [175] T. Binninger, A. Marcolongo, M. Mottet, V. Weber, T. Laino, *J. Mater. Chem. A* **2020**, *8*, 1347–1359.
- [176] Y. Zhu, X. He, Y. Mo, *ACS Appl. Mater. Interfaces* **2015**, *7*, 23685–23693.
- [177] Z. Deng, Z. Wang, I.-H. Chu, J. Luo, S. P. Ong, *J. Electrochem. Soc.* **2015**, *163*, A67.
- [178] Y. Wu, S. Wang, H. Li, L. Chen, F. Wu, *InfoMat* **2021**, *3*, 827–853.
- [179] Y. Li, X. Chen, A. Dolocan, Z. Cui, S. Xin, L. Xue, H. Xu, K. Park, J. B. Goodenough, *J. Am. Chem. Soc.* **2018**, *140*, 6448–6455.
- [180] A. Sakuda, A. Hayashi, M. Tatsumisago, *Sci. Rep.* **2013**, *3*, 2261.
- [181] C. Monroe, J. Newman, *J. Electrochem. Soc.* **2005**, *152*, A396.
- [182] C. Brissot, M. Rosso, J.-N. Chazalviel, S. Lascaud, *J. Power Sources* **1999**, *81*, 925–929.
- [183] J. Wolfenstine, J. L. Allen, J. Sakamoto, D. J. Siegel, H. Choe, *Ionics* **2018**, *24*, 1271–1276.
- [184] A. Kato, M. Nose, M. Yamamoto, A. Sakuda, A. Hayashi, M. Tatsumisago, *J. Ceram. Soc. Jpn.* **2018**, *126*, 719–727.
- [185] S. Pugh, *London Edinburgh Philos. Mag. J. Sci.* **1954**, *45*, 823–843.
- [186] R. Sudo, Y. Nakata, K. Ishiguro, M. Matsui, A. Hirano, Y. Takeda, O. Yamamoto, N. Imanishi, *Solid State Ionics* **2014**, *262*, 151–154.
- [187] C.-L. Tsai, V. Roddatis, C. V. Chandran, Q. Ma, S. Uhlenbruck, M. Bram, P. Heitjans, O. Guillou, *ACS Appl. Mater. Interfaces* **2016**, *8*, 10617–10626.
- [188] T. Krauskopf, R. Dippel, H. Hartmann, K. Peppler, B. Mogwitz, F. H. Richter, W. G. Zeier, J. Janek, *Joule* **2019**, *3*, 2030–2049.
- [189] J. T. Warner, *Lithium-Ion Battery Chemistries: A Primer*, Elsevier, Amsterdam, **2019**.
- [190] L. Miara, A. Windmüller, C.-L. Tsai, W. D. Richards, Q. Ma, S. Uhlenbruck, O. Guillou, G. Ceder, *ACS Appl. Mater. Interfaces* **2016**, *8*, 26842–26850.
- [191] E. Yi, W. Wang, J. Kieffer, R. M. Laine, *J. Mater. Chem. A* **2016**, *4*, 12947–12954.
- [192] H. Geng, K. Chen, D. Yi, A. Mei, M. Huang, Y. Lin, C. Nan, *Rare Metal Mater. Eng.* **2016**, *45*, 612–616.
- [193] M. Huang, T. Liu, Y. Deng, H. Geng, Y. Shen, Y. Lin, C.-W. Nan, *Solid State Ionics* **2011**, *204*, 41–45.
- [194] L. Xu, S. Tang, Y. Cheng, K. Wang, J. Liang, C. Liu, Y.-C. Cao, F. Wei, L. Mai, *Joule* **2018**, *2*, 1991–2015.
- [195] A. Banerjee, X. Wang, C. Fang, E. A. Wu, Y. S. Meng, *Chem. Rev.* **2020**, *120*, 6878–6933.
- [196] K. J. Kim, J. L. Rupp, *Energy Environ. Sci.* **2020**, *13*, 4930–4945.
- [197] F. Han, J. Yue, C. Chen, N. Zhao, X. Fan, Z. Ma, T. Gao, F. Wang, X. Guo, C. Wang, *Joule* **2018**, *2*, 497–508.
- [198] G. V. Alexander, N. C. Rosero-Navarro, A. Miura, K. Tadanaga, R. Murugan, *J. Mater. Chem. A* **2018**, *6*, 21018–21028.
- [199] Y.-N. Yang, Y.-X. Li, Y.-Q. Li, T. Zhang, *Nat. Commun.* **2020**, *11*, 5519.
- [200] S. Ohta, J. Seki, Y. Yagi, Y. Kihira, T. Tani, T. Asaoka, *J. Power Sources* **2014**, *265*, 40–44.
- [201] Z. Zhao, Z. Wen, X. Liu, H. Yang, S. Chen, C. Li, H. Lv, F. Wu, B. Wu, D. Mu, *Chem. Eng. J.* **2021**, *405*, 127031.
- [202] G. Zhong, C. Wang, R. Wang, W. Ping, S. Xu, H. Qiao, M. Cui, X. Wang, Y. Zhou, D. J. Kline, *Energy Storage Mater.* **2020**, *30*, 385–391.
- [203] X. Han, S. Wang, Y. Xu, G. Zhong, Y. Zhou, B. Liu, X. Jiang, X. Wang, Y. Li, Z. Zhang, *Energy Environ. Sci.* **2021**, *14*, 5044–5056.
- [204] X. Li, Z. Ren, M. Norouzi Banis, S. Deng, Y. Zhao, Q. Sun, C. Wang, X. Yang, W. Li, J. Liang, *ACS Energy Lett.* **2019**, *4*, 2480–2488.
- [205] S. P. Culver, R. Koerver, W. G. Zeier, J. Janek, *Adv. Energy Mater.* **2019**, *9*, 1900626.
- [206] J. Liang, Y. Sun, Y. Zhao, Q. Sun, J. Luo, F. Zhao, X. Lin, X. Li, R. Li, L. Zhang, *J. Mater. Chem. A* **2020**, *8*, 2769–2776.
- [207] X. Yang, Q. Yin, C. Wang, K. Doyle-Davis, X. Sun, X. Li, *Prog. Mater. Sci.* **2023**, *140*, 101193.
- [208] Y. Luo, X. Yang, C. Wang, A. Fraser, H. Zhang, X. Sun, X. Li, *Prog. Mater. Sci.* **2023**, *139*, 101171.
- [209] H. Huo, Y. Chen, N. Zhao, X. Lin, J. Luo, X. Yang, Y. Liu, X. Guo, X. Sun, *Nano Energy* **2019**, *61*, 119–125.
- [210] H. Huo, J. Luo, V. Thangadurai, X. Guo, C.-W. Nan, X. Sun, *ACS Energy Lett.* **2019**, *5*, 252–262.
- [211] Y. Liu, C. Li, B. Li, H. Song, Z. Cheng, M. Chen, P. He, H. Zhou, *Adv. Energy Mater.* **2018**, *8*, 1702374.
- [212] J. Zhu, X. Li, C. Wu, J. Gao, H. Xu, Y. Li, X. Guo, H. Li, W. Zhou, *Angew. Chem. Int. Ed.* **2021**, *60*, 3781–3790.
- [213] H. Wang, C. Yu, S. Ganapathy, E. R. van Eck, L. van Eijck, M. Wagemaker, *J. Power Sources* **2019**, *412*, 29–36.
- [214] P. He, Y. Tang, Z. Tan, C. Lei, Z. Qin, Y. Li, Y. Li, Y. Cheng, F. Wu, Z. He, *Nano Energy* **2024**, *124*, 109502.

Manuscript received: October 14, 2024

Revised manuscript received: November 5, 2024

Accepted manuscript online: November 7, 2024

Version of record online: November 22, 2024